Title
Rapid Isolation and Biophysical Characterization of Circulating Tumor Cells with Microfluidic Vortex Technology

Author
Che, James

Publication Date
2015

Peer reviewed|Thesis/dissertation

UNIVERSITY OF CALIFORNIA

Los Angeles

Rapid Isolation and Biophysical Characterization of Circulating Tumor Cells with Microfluidic Vortex Technology

A disseration submitted in partial satisfaction of the

requirements for the degree Doctor of Philosphy

in Bioengineering

by

James Che

2015

ABSTRACT OF THE DISSERTATION

Rapid Isolation and Biophysical Characterization of

Circulating Tumor Cells with Microfluidic Vortex Technology

by

James Che

Doctor of Philosophy in Bioengineering

University of California, Los Angeles, 2015

Professor Dino Di Carlo, Chair

Disseminated and circulating tumor cells are key players of metastatic cancer and have high diagnostic and prognostic value. These cells may often accumulate and persist in body fluids—such as in pleural effusions or blood—which are minimally-invasive sources for patient sampling. However, tumor cells are relatively scarce and must typically be enriched from a large background of blood cells. An inertial microfluidic device was developed to specifically trap and concentrate large tumor cells in stable microvortices which form under high flow rates. The novel label-free Vortex platform was optimized to isolate large rare cells at high efficiency (up to 80%), purity (10-80%), concentration (~200 μL volume), and viability (>80%) in a short time period (<30 min). Enriched cells from pleural effusions and blood are made freely available and compatible for a variety of downstream analysis techniques.

This work highlights the purification of disseminated tumor cells from pleural effusions, yielding i) a greater than 65-fold enrichment of malignant cells for a significant reduction in cytology slide background that facilitates ease of diagnostics by pathologists, and ii) an increase in area under the receiver operating characteristic curve from 0.90 to 0.99 for the detection of point mutations which may aid in personalized medicine. Isolation of circulating tumor cells from blood was also demonstrated and applied toward i) immunofluorescent staining to achieve a 5.7x higher success rate of tumor cell detection than the existing CellSearch gold standard, and ii) mechanophenotyping of cells by deformability as a truly label-free and potentially superior approach over immunostaining (93.8% vs. 71.4% success rate) for enriching and enumerating cells to determine cancer patient prognosis. The presented platform technology is a means for rapidly providing valuable information about patient state that is useful for informed cancer treatments and monitoring of disease progression.

The dissertation of James Che is approved.

Amy C. Rowat

Pei-Yu Chiou

Jian Yu Rao

Dino Di Carlo, Committee Chair

University of California, Los Angeles

2015

DEDICATION

I would like to dedicate this work to my loving mother, who has the purest, strongest heart in the world, and my loving father, the greatest role model a son could ever ask for. I would also like to recognize my advisor and all my lab-mates who have been such positive influences behind my research and have helped fuel my ambition to conduct meaningful work, and my friends who have helped maintain my sanity outside the laboratory setting and made my graduate experience the most fulfilling part of my life thus far. Finally, I dedicate this work to those affected by cancer; despite my brief encounters with patients in the clinic, it is through those emotional interactions that I have been motivated to pursue clinically practical technology which may one day help alleviate such significant disease burdens in healthcare.

TABLE OF CONTENTS

ACKNOWLEDGEMENTS

Chapter 1 includes portions from the publication: [Sollier E, Go DE, Che J, Gossett DR, O'Byrne S, Weaver WM, Kummer N, Rettig M, Goldman J, Nickols N, McCloskey S, Kulkarni RP, and Di Carlo D (2014) "Size-selective collection of circulating tumor cells using Vortex technology". Lab on a Chip, 14, 63-77. doi: 10.1039/C3LC50689D]. ES, DEG, and JC performed experiments, analyzed data, and prepared the manuscript. DRG, SO, and WMW provided aid for experimental setups. NK, MR, JG, NN, and SM provided patient samples and guidance on the work. RP and DD provided guidance throughout the work and manuscript.

Chapter 2 is adapted from: [Che J, Mach AJ, Go DE, Talati I, Ying Y, Rao J, Kulkarni RP, and Di Carlo D (2013) "Microfluidic purification and concentration of malignant pleural effusions for improved molecular and cytomorphological diagnostics". PLoS ONE. 8(10):e78194. doi: 10.1371/journal.pone.0078194]. JC, AJM, DEG, and IT performed experiments and analyzed data. YY and JR provided clinical samples and inputs for the manuscript. RP and DD provided guidance throughout the work and manuscript.

The author and work was supported by funding from the Coulter Foundation Translational Research Award (Grant #N00014-12-1-0847), the Office of Naval Research Young Investigator Program (Grant #20101030), the National Institutes of Health Innovative Molecular Analysis Technologies Program (Grant #5R33CA177456), and a sponsored research grant with NetScientific.

VITA

PREVIOUS EDUCATION

M.S. Biomedical Engineering (2014), University of California, Los Angeles

B.S. Bioengineering (2011), University of California, Berkeley

RESEARCH APPOINTMENTS

01/12 – 12/15 Graduate Student Researcher, University of California, Los Angeles

Professor Dino Di Carlo, Microfluidic Biotechnology

01/11 – 05/11 Undergraduate Student Researcher, University of California, Berkeley

Professor Amy Herr, Bioinstrumentation for Quantitative Biology & Medicine

01/08 – 05/10 Research Assistant, University of California, Berkeley

Professor Mimi Koehl, Ecological and Evolutionary Biomechanics

WORK EXPERIENCE

06/12 – 09/14 Assistant Learning Skills Counselor, University of California, Los Angeles

High School Summer Research Program, Henry Samueli School of Eng.

01/12 – 06/12 Teaching Assistant, University of California, Los Angeles

Bioengineering 167L (03/12–06/12), Chemistry 14A (01/12–03/12)

05/10 – 08/10 Quality Intern, Abbott Laboratories, Waukegan, IL

Human Factors Research, Abbott Quality and Regulatory

PUBLICATIONS

1. Che J, Yu V, Goldman J, et. al. "Rapid isolation and biophysical characterization of circulating tumor cells" (in progress)
2. Che J, Yu V, Dhar M, et. al. "Classification of large circulating tumor cells isolated with ultra-high throughput microfluidic Vortex technology." (in review)

3. Che J, Mach AJ, Go DE, et. al. (2013). "Microfluidic purification and concentration of malignant pleural effusions for improved molecular and cytomorphological diagnostics." PLoS ONE. 8(10):e78194.
4. Sollier E, Go DE, Che J, et. al. (2014). "Size-selective collection of circulating tumor cells using Vortex technology." Lab on a Chip. 14:63-77.

PRESENTATIONS

1. Che J, Yu M, Di Carlo D. "An integrated platform for label-free isolation and mechanophenotyping of circulating tumor cells." Poster presentation at MicroTAS. 2015 October 25-29; Gyeongju, South Korea.
2. Che J, Dhar M, Yu V, et. al. "Ultra-high throughput isolation of circulating tumor cells with microfluidic Vortex technology." Poster presentation at MicroTAS. 2014 October 26-30; San Antonio, TX.
3. Che J, Sollier E, Go DE, et al. "Microfluidic vortex technology for pure circulating tumor cell concentration from patient blood." Poster presentation at MicroTAS. 2013 October 26-31; Freiburg, Germany.
4. Che J, Mach AJ, Go DE, et. al. "Microfluidic Sample Preparation of Pleural Effusions for Cytodiagnostics." Oral presentation at Biomedical Engineering Society Annual Meeting. 2012 October 24-27; Atlanta, GA.

HONORS AND AWARDS

CBMS Student Travel Grant (MicroTAS 2014, San Antonio, TX)

Cheminas Young Researcher Poster Award (MicroTAS 2013, Freiburg, Germany)

Cheminas Poster Award (MicroTAS 2012, Okinawa, Japan)

Chapter 1: Microfluidic Isolation of Rare Tumor Cells

Disseminated and circulating tumor cells

In patients with metastatic cancer, cells shed from a primary tumor to distant sites in the body in the form of disseminated tumor cells (DTCs). It is this metastatic process of spread and growth which may disrupt normal physiological function, leading to 90% of cancer-related deaths and totalling up to 500,000 deaths per year in the United States [1]. While DTCs are known to spread to different organ systems, they may also accumulate and persist in body fluids, such as pleural or perotineal fluids (Fig. 1.1).

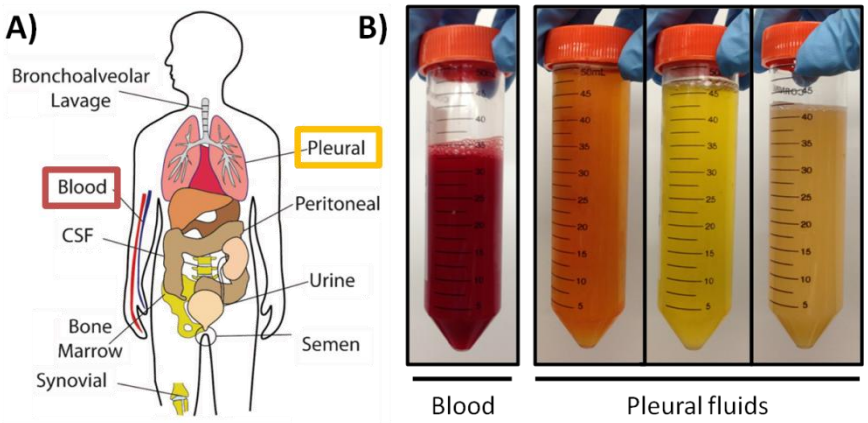

Figure 1.1: Types of fluids in the body. (A) Disseminated tumor cells may accumulate at various fluid sites in patients with metastatic cancer. Adapted from Mach et. al. (*Lab Chip*, 2011). (B) The presented work examines tumor cells from blood and pleural fluids, which range in cellular and fluidic consistency between patients.

DTCs from body fluids are minimally invasive and convenient sources of patient sampling that may elucidate more information about patient state. For example, the cells may be used for molecular analysis, especially for personalized cancer therapies [2]. An emerging trend in cancer therapy is the use of pharmacological agents that target specific molecular pathways affected by common genetic lesions [3, 4]. These drugs are only effective in patients who have tumors with the specified molecular lesions, and drug efficacy can also drop due to the emergence of resistance associated with peripheral or secondary mutations. As a result, drug

treatments must be individualized following the molecular analysis of the tumor, by detecting the presence of particular sensitivity mutations or drug-resistance mutations [3, 5-7]. In some cases the primary tumor may be biopsied to analyze cancer cells, but it may often be inaccessible or have been surgically removed, necessitating CTCs as an alternative source for tumor cells.

DTC isolation and analysis is also crucial for cancer research and may unveil the mechanisms in which secondary tumor sites form [2]. Greater understanding of cancer malignancy would impact the translation of cancer research toward the therapeutic benefit of patients, as it would enable new preventative approaches with the discovery of new biomarkers. Extensive studies on the mechanisms of metastasis suggest that a large molecular and cellular heterogeneity exists among CTCs, for different patients with the same type of cancer or even among the cancer cells of the same patient [8, 9], and results have all emphasized that metastasis is a complex multi-step process which is still largely unknown [10].

Of particular interest are the types of DTCs found in blood, known as circulating tumor cells (CTCs), which play a major role in metastasis (Fig. 1.2) [11]. It has been shown that the relative number of CTCs in blood correlates with patient prognosis, in which a large number corresponds with poor patient outcome and lowered chance of survival [12]. Therefore, routine isolation and enumeration of CTCs from blood is needed to determine patient prognosis and potentially assess treatment efficacy [13]. Such analyses of a "liquid biopsy" may be more effective at detecting early tumor resistance and regrowth than traditional CT and/or PET scans, which are conducted less frequently due to cost and radiation concerns [14].

However, both DTCs and CTCs are often very rare, occurring at concentrations as low as 1-10 CTCs per mL of whole blood, in a background of millions of white blood cells (WBCs) and billions of red blood cells (RBCs) [11]. With such clinical need and relevance, this iconic

biological "needle in a haystack" type of challenge has now become a burgeoning field for biotechnological innovation towards extremely sensitive detection of rare cells. In order to be clinically practical, cells must ideally be isolated from one tube of sample with high efficiency and throughput, while outputting a sample high in purity.

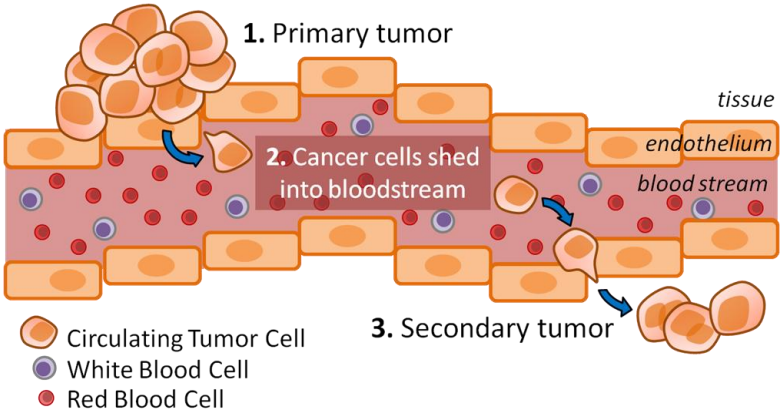

Figure 1.2: Circulating tumor cells. CTCs shed from a tumor and into the blood stream, where they may travel and spread to distant sites in the body. CTCs in patients with metastatic cancer are typically found at extremely low concentrations in the blood and are hidden in a large background of leukocytes and erythrocytes.

Technologies for rare cell isolation

Microfluidic technology is an emerging tool that may deliver automated, well-controlled micron-scaled systems to purify target cells with the highest possible sensitivity and specificity. The ability to distinguish DTCs from non-DTCs is essential for isolation and detection, and emerging technologies attempt to take advantage of unique cellular properties. For example, dielectrophoresis (ApoCell) and acoustophoresis (CellCare) target the electrical and compressibility properties, respectively, of cancer cells. However, the throughput of these approaches is still low, and both require a preliminary lysis of blood to reduce the significant cellular background, which may agitate or damage native DTCs [15,16].

Alternatively, isolation may be performed using affinity-based capture methods to take advantage of unique tumor cell surface properties [17]. Antibodies or aptamers which target

surface antigens such as epithelial cell adhesion marker (EpCAM) or cytokeratin (CK) have been utilized to bind and separate CTCs, either by functionalized microchannel surfaces or magnetic particles. The CellSearch system (Janssen Diagnostics) is the current FDA-approved gold standard prognostic tool which makes use of a ferromagnetic immunoaffinity assay that targets CTCs using anti-EpCAM probes [18,19]. Despite high capture efficiencies using cell lines, it remains challenging to capture all patient sample CTCs, due to high cell-to-cell heterogeneity in which cells are now known to undergo an epithelial-to-mesenchymal transition (EMT) that downregulates target epithelial cell surface markers in favor of a more mobile, invasive mesenchymal phenotype [20,21].

Finally, cell size is another property that distinguishes tumor cells, as DTC diameters for a range of cancer types (carcinomas, sarcomas and melanoma) have been shown to be 2-3 times larger (>15 μm) than normal red blood cells (~6-8 μm) and oftentimes larger than white blood cells (12-15 μm); this size-based distinction has been exploited for several CTC isolation technologies [22,23]. Cote et al. have used a method to trap these larger cells using precisely microfabricated filters. Although microfiltration is a simple and straightforward approach, CTCs are highly deformable and are able to squeeze through filter pores unless they are stiffened by chemical fixation [24,25]. As a result of fixation, cells cannot be used for downstream live-cell application such as metabolomics or cell culture. Other filter alternatives, such as ScreenCell [26] or ISET [23,27,28], do not require preliminary cell fixation and constitute an attractive and simple approach for CTC counting, and microfluidic approaches further refine the interaction between cells and microfabricated structures [29,30], including the use of microchannel constrictions [31], micropillar arrays [32], and other microfilter variations [33-36]. However, direct filtration approaches are prone to clogging, and cells may be difficult to release for further

downstream analysis. To overcome these additional concerns, as partly defined as one of the "Grand Challenges of the LOC Community" by J. den Toonder in 2011 [37], a size-based purely hydrodynamic approach is still needed for high-purity and high-throughput extraction of viable CTCs from a large volume of blood.

Continuous flow microfluidics has more recently gained traction as a promising technology for the reduced-contact isolation and extraction of viable CTCs by size, such as hydrodynamic filtration [38,39] or deterministic lateral displacement [40,41]. Additionally, advances in inertial microfluidics have offered a more rapid platform through which cells may be sorted by size, as fluidic forces generated from high flow rates scale strongly with cell size [42-44]. Notable technologies with high capture efficiencies include the use of shear gradient lift forces in expansion-contraction microchannels [45-47], Dean vortices in spiral microfluidic chips (Clearbridge Biomedics, Hou et. al.) [48-50], and inertial focusing prior to WBC depletion using immunomagnetic beads (CTC-iChip, Toner et. al.) [51]. Despite relatively higher throughputs, current techniques have been hindered by scalability, low sample purity, and dilute output sample volumes which require additional cell concentration steps. The ideal technology provides continuous, efficient, high-throughput, simple, and pure collection of viable CTCs from large volumes of blood samples.

Size-based isolation with Vortex technology

Vortex technology is a high-throughput microfluidic "filter-less filter" platform that has recently been developed to passively trap and concentrate cells in microvortices based on size. Vortex devices operate at high flow rates and require an understanding of inertial forces and focusing. As first experimentally visualized by Segre and Silberberg in 1961 and more recently characterized by Di Carlo and others, inertial focusing makes use of high Reynolds number flow

profiles to align microparticles and cells within microchannels [52-54]. Randomly dispersed particles flowing in an enclosed channel with particle Reynolds number (Re_P) > 1 are subjected to two counteracting inertial lift forces: i) a shear-gradient lift force F_{LS}, scaling as $F_{LS} = f_L \rho U_m^2 a^3 / W_C$ that directs particles toward the channel walls, and ii) a wall effect lift force F_{LW}, scaling as $F_{LW} = f_L \rho U_m^2 a^6 / W_C^4$, that is due to the presence of the wall and repels the particles toward the channel centerline [52]. $Re_P = Re(a/W_C)^2$ where a/W_C is the ratio of particle diameter to the channel width, and Re is channel Reynolds number $Re = \rho U_m D/\mu$, the ratio of inertial to viscous effects. Here D is the hydraulic diameter of the channel, U_m is the maximum velocity of the fluid with density ρ and dynamic viscosity μ, while f_L is the dimensionless lift coefficient.

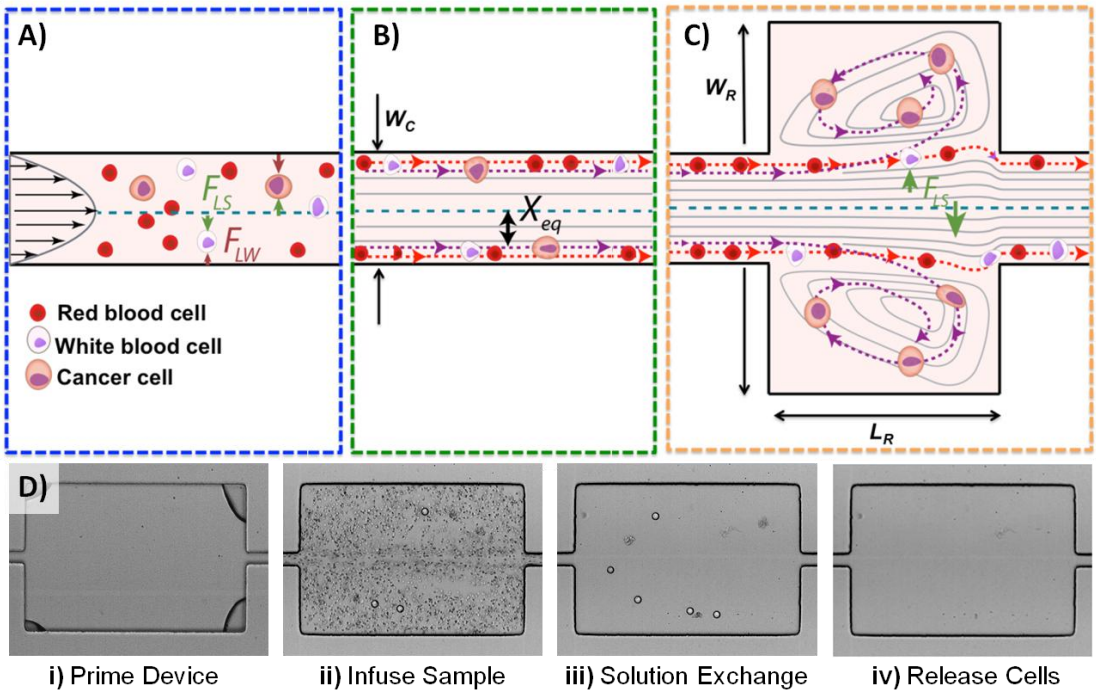

Figure 1.3: Vortex trapping mechanism. (A) At the channel inlet, cells are randomly distributed and experience opposing wall effect F_{LW} and shear-gradient F_{LS} lift forces. **(B)** As a result, particles migrate to dynamic lateral equilibrium positions, X_{eq}, depending on the channel cross section. **(C)** Upon entrance into the reservoir, the wall effect becomes negligible. Larger cells (violet dashed line) continue to experience a large F_{LS} and are driven away from the channel center, through the separatrix, and into the vortices. Large cells become stably trapped, while smaller cells (red dashed line) do not experience enough F_{LS} to become entrained in stable orbits and exit in the main flow. **(D)** The typical workflow for Vortex processing requires device priming, sample infusion, solution exchange, and cell release.

The key aspect of Vortex technology is the use of rectangular reservoirs along the path of straight narrow channels which form stable microvortices at high flow rate and *Re* (Fig. 1.3). An inertial boundary layer separation accounts for these predictable laminar vortices (i.e. Moffatt corner eddy flow) that occur at the sudden expansions in the main channels [55,56]. As cells first focus toward the two lateral walls of the straight channel and enter the expanding reservoir, the wall effect lift force becomes negligible. The dominating shear gradient lift force F_{LS} then dominates and causes particles to migrate across fluid streamlines, pass the separatrix (i.e. the boundary between the main flow and the secondary vortex patterns), and enter the recirculating vortex region. Since shear-gradient lift forces scale with a^3, larger particles experience a larger lateral lift that may be sufficient for stable vortex trapping, while smaller cells either remain in the main stream or are unstably trapped in the reservoirs and escape the vortex after several orbits (Fig. 1.3C). Microfluidic geometries and flow parameters are tuned to selectively isolate the larger tumor cells, while smaller red and white blood cells are depleted from the sample. Tumor cells are stably trapped and accumulate over time as more volume is processed. Stable entrapment also allows for a solution exchange at the same flow rate to wash away unstably trapped smaller particles, and all cells may be released in a concentrated low volume simply by lowering the flow rate to dissipate the vortices.

Fabrication and standard operation of Vortex devices

Conventional polydimethylsiloxane (PDMS) replica molding processes were used to assemble Vortex devices [57]. Microfluidic channels were designed using AutoCAD (Autodesk Inc.) and printed on a 20,000 dpi photomask (CAD/Art Services, Inc.). A master mold was fabricated with the mask and standard photolithographic techniques using negative KMPR 1050 i-line photoresist (MicroChem Corp.) on a 4-inch silicon wafer (University Wafer, Inc.). Specific

photoresist spin speeds and exposure (Karl Suss MA6, SUSS MicroTec), development (SU-8 developer, MicroChem Corp), and baking times were adjusted according to the manufacturer datasheet (MicroChem Corp.) to achieve desired microchannel heights. Master mold height was confirmed using a profilometer (Veeco Metrology). PDMS was mixed in a 1:10 curing agent-to-base ratio, degassed, and cured over the mold at 65°C for 21 hours. PDMS was then cut, peeled from the wafer mold, and hole-punched (Syneo, LLC) before bonding to 3"x1" glass slides (VWR International LLC) using oxygen plasma (800 Micro RIE, Technics, Inc.) at 500 mTorr and 80 W of radio frequency power for 30 s. Devices were maintained at 65°C in an oven for over 15 min to increase bonding.

Several key parameters are critical for the evaluation of rare cell isolation devices. Device efficiency is defined as the number of captured target particles over the total number of target particles processed through the device. Sample purity represents the number of target particles in the sample over the total number of particles in the sample, and sample enrichment is defined as the ratio of sample purity after device processing to the sample purity before processing. Over the course of the presented work, MCF7 breast cancer cells (ATCC) were used to characterize device efficiency. Cells were cultured in an incubator at 37°C and 5% CO_2 with minimum essential medium supplemented with 10% fetal bovine serum, 1% penicillin-streptomycin-glutamine, and 0.01 mg/mL human recombinant insulin (Gibco). Adherent cells were released with 0.25% (w/v) trypsin (Gibco), resuspended in media, assessed for concentration with a hemocytometer, and rocked gently on a shaker 30 min prior to experiments. For efficiency tests, a low target number of ~300 cells was spiked in 4 mL of PBS or diluted healthy blood, infused through the device, collected in a well plate, and compared with a control well containing the same number of initial cells. Flow was typically driven by the use of two syringe pumps

(Harvard Apparatus), one for the sample solution and one for the wash solution. Devices were initially primed with wash buffer at high flow rate for 30 s before switching to sample infusion at the same flow rate (Fig. 1.3D). After cell capture, the sample flow was stopped and wash flow was started at the same flow rate to perform a solution exchange for ~15 s. Finally, all flow was stopped to dissipate vortices and release target cells, which were collected in a 96-well plate (Greiner CELLSTAR) for imaging and enumeration.

Cells collected for enumeration were fixed in 2% paraformaldehyde (Electron Microscopy Sciences) for 10 min, permeabilized in 0.4% v/v Triton X-100 (Research Products International Corp) for 7 min, blocked with 5% goat serum (Invitrogen) for 30 min, and stained with DAPI (nucleus, Molecular Probes), anti CD45-phycoerythrin (CD45-PE for WBCs, Clone HI30, BD Biosciences), and a fluorescein isothiocyanate (FITC)-conjugated anti cytokeratin (CK, epithelial cells) cocktail for Pan-CK AE1/AE3 (eBioscience), CK3-6H5 (Miltenyi Biotec), and CK CAM5.2 (BD Biosciences). Stitched images of stained wells were acquired at 100x magnification (Zeiss Axio Observer Z1 microscope with ZEN software and Photometrics CoolSnap HQ2 CCD camera), and cells from clinical samples were manually enumerated by 2 different persons who were blinded to avoid bias. Several key parameters are critical for the evaluation of rare cell isolation devices. Device efficiency is defined as the number of enriched target particles over the total number of particles processed through the device. Sample purity represents the fraction of target cells in the sample, and sample enrichment is defined as the ratio of sample purity after device processing to the sample purity before processing.

Empirical testing for understanding of Vortex trapping

While traditional microfluidic devices may often be optimized using software simulations, it is computationally difficult to model Vortex devices due to the high operating

Reynolds number, in which both viscous and inertial effects dynamically influence concentrated particles in a three-dimensionally complex environment. As a result, several comprehensive empirical tests were performed to gain more insight about the nature of Vortex trapping.

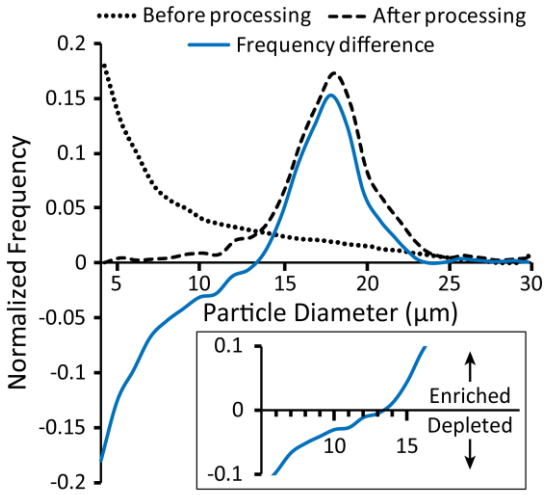

Figure 1.4: Vortex size cutoff. Polydisperse PDMS beads (4-30 µm diameter) were processed through the Vortex HT device. The normalized frequency distribution of unprocessed beads (dotted line) was subtracted from the normalized frequency of captured beads (dashed line) to portray particle size selectivity (solid line). Bead sizes with normalized frequency differences below 0 represent size ranges which are depleted from a sample, whereas those above 0 (> ~13 µm) are favored to be captured and enriched by Vortex HT.

First, vortex trapping favors large particles. Using a 40 µm width main channel with 480×720 µm reservoir size and *Re* = 150, the vortex chambers demonstrate selective enrichment for particles greater than ~13 µm, among a polydisperse solution of deformable PDMS microbeads (Fig. 1.4). Since larger particles experience larger shear gradient lift forces, the stability of orbits may be more stable, as larger particles also exhibit smaller orbits that are tighter towards the core of the vortex [58]. While large single particles exhibit stable, consistent orbits, particle trajectories fluctuate and are altered in the presence of more particles due to particle-particle interactions (Figs. 1.5A-1.5B). Resulting fluctuations in trajectories may cause instability and loss of trapped particles. In terms of dense fluids like blood, in which ~45% of fluid volume consists of small blood cells, particle interactions may thus greatly limit trapping

efficiency of CTCs. Dilution of blood in a buffer solution (PBS) prior to sample processing helps to i) lower particle concentration and minimize such interactions, and ii) lower fluid viscosity, resulting in increased stability and efficiency (Fig. 1.5C). While it is a trade-off between efficiency and throughput, a dilution factor of 10X was chosen as a standard for subsequent clinical sample processing with blood.

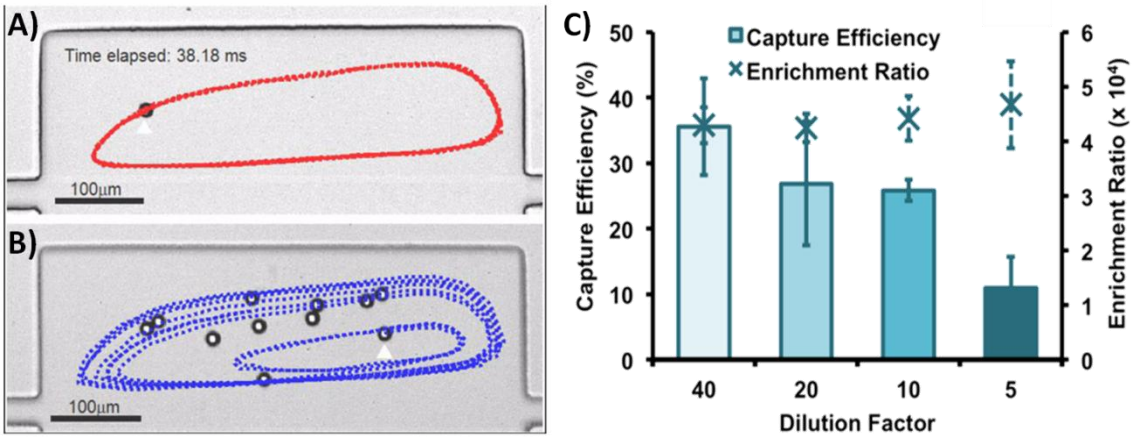

Figure 1.5: Effect of particle concentration on Vortex trapping. A particle trajectory is shown traced over the course of ~38 ms in the conditions of **(A)** no other particles and **(B)** several particles trapped in the same reservoir. Orbits changes from a single stable trajectory to a fluctuating trajectory due to particle-particle interactions. **(C)** Diluting blood (5X-40X in PBS) decreases particle concentrations and lowers interactions to improve the stability and efficiency of Vortex trapping.

Next, particle capture is affected by Reynolds number (Fig. 1.6). At low flow rates and *Re*, either vortices are not fully developed (Fig. 1.6A), or fluid shear gradient lift is not sufficient to efficiently trap particles (Fig. 1.6B). At very high Reynolds numbers (*Re* > 200), the vortex core shifts toward the rear end of the reservoirs, and orbiting particles begin to collide with the back wall (Fig. 1.6D), which may destabilize orbits and lower capture efficiency. An optimal flow rate is one in which the vortex occupies the entire reservoir and achieves a balance between shear gradient lift and the time and distance to cross fluid streamlines for maximum capture efficiency (Fig. 1.6C). Further testing also reveals that optimal trapping occurs at different flow rates for rigid beads versus more deformable cells of similar diameter (Fig. 1.6E).

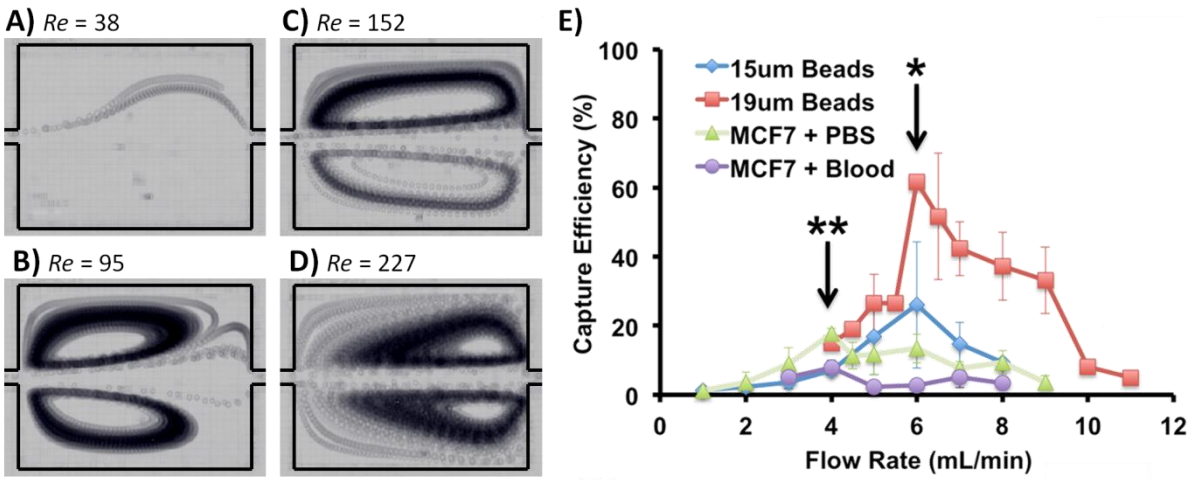

Figure 1.6: Effect of flow rate on Vortex trapping. **(A)-(D)** Particle traces are shown for varying flow rates moving from left to right, ranging from low (*Re* = 38) to high (*Re* = 227). The position of the vortex center moves from the entrance of the reservoir toward the rear as *Re* increases. **(E)** Maximum capture efficiency occurs at different flow rates for different particles.

Particle capture is also affected by the length of the upstream straight channel before the vortex reservoir (Fig. 1.7). Tests with 20 μm beads revealed a peak efficiency using a 500 μm upstream distance before reservoirs, below which efficiency decreases (Fig. 1.7A). Corresponding COMSOL software simulations reveal that fluid velocity profiles only become fully developed after a minimum 500 μm distance, which suggests that the shear gradient lift force needed to trap particles is not sufficient for reservoirs spaced too closely together. Thus, although increasing upstream channel length increases the fluid pressure required to drive flow at the required high *Re* (i.e., risking device delamination or bursting), some distance is required to obtain efficient particle trapping.

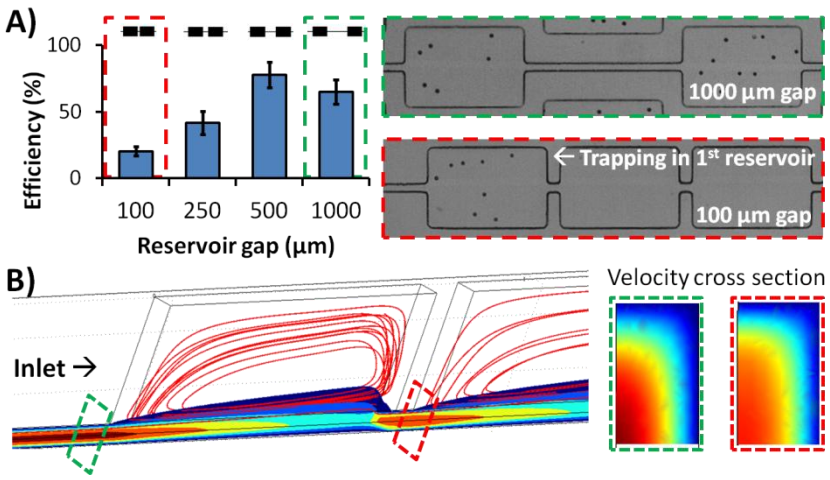

Figure 1.7: Effect of upstream channel length on Vortex trapping. **(A)** Devices with serial reservoirs of varying gaps were tested for efficiency. Efficiencies drop below a 500 µm spacing. For devices with a 100 µm spacing, particles were only observed in the first reservoir, which contained a longer upstream channel length. **(B)** COMSOL simulations show that the fluid shear gradient in the main channel shortly after each reservoir (dotted red) has not yet fully developed. A minimum distance of 500 µm is sufficient to achieve fully developed flow(dotted green).

Finally, vortex isolation by size allows large cells from different cancer types to be trapped. Tests with cell lines from melanoma (M395) and ovarian (OVCAR5), breast (MCF7), lung (A549), and prostate (PC3) cancer spiked in 10X diluted healthy blood confirms successful trapping (Fig. 1.8A). Capture is independent of the level of cell surface antigen expression, with MCF7 and OVCAR5 having high EpCAM expression (around 500,000 antigens/cell) [59, 60], PC3 with medium expression (50,000 antigens/cell) [59], A549 with low expression [61], and finally M395 which are not of epithelial origin. Large cell lines (MCF7 and M395, both 17.7 µm average diameter) generally displayed higher capture efficiencies. However, large PC3 cells (18.2 µm) exhibited lower capture efficiency, which is likely due to their high deformability.

Work by Hur et al. showed that more deformable particles are inertially focused at equilibrium positions closer to the channel center [62] and this could address the inconsistent correlation between capture efficiencies of similarly sized cells. More deformable cells will be focused further away from the vortices and may not experience shear gradient lift forces large

enough to cross the separatrix. Indeed, MCF7 cells (avg. 18.9 μm) were less deformable (median 1.6) than M395 cells of similar size (19.3 μm, 1.9 median deformability) but displayed a greater capture efficiency (26.4% vs. 19.4%, Fig. 1.8B).

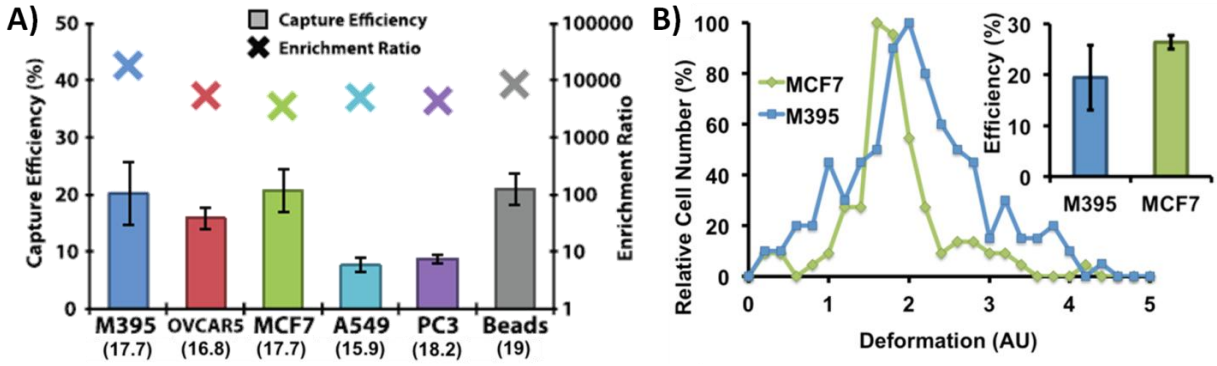

Figure 1.8: Vortex trapping applies to many cancer types. **(A)** Cells from melanoma and ovarian, breast, lung, and prostate cancers demonstrated capture at different efficiencies. Large cell lines tended to exhibit larger capture efficiency. Enrichment ratios tended to remain consistent at 10^4 fold enrichment. Average cell size in microns is shown below each cell line. **(B)** Vortex trapping efficiency is lowered by increasing cell deformability. M395 cells are similar in size to MCF7 cells, but are more deformable and thus exhibit a lower efficiency. Deformability measurements were carried out with Deformability Cytometry devices developed by Gossett et. al. [63].

Opportunities for clinical applications

The vortex trapping approach has particular advantages. A short processing time, high concentration ratio, applicability to various sample and cancer types, cell integrity, and high-purity are especially important for clinical adoption and use in downstream assays. In the subsequent chapters, the progression of key microfluidic Vortex designs will be presented, along with their clinical applications in cytopathology, genetic analysis, immunofluorescent staining, and cellular mechanophenotyping of rare tumor cells found in both pleural effusions and blood.

References

[1] American Cancer Society. *Cancer Facts and Figures 2015*. Atlanta: American Cancer Society; 2015.

[2] K. Pantel, C. Alix-Panabieres, Circulating tumor cells in cancer patients: challenges and perspectives. *Trends in Molecular Medicine*, 2010, **16,** 398-406.

[3] S. Riethdorf, V. Muller, L. Zhang, T. Rau, S. Loibl, M. Kinor et al., Detection and HER2 expression of circulating tumor cells: prospective monitoring in breast cancer patients treated in the neoadjuvant GeparQuattro trial, *Clin. Cancer Res.*, 2010, 16, **9,** 2634-2645.

[4] M. Méndez, A. Custodio and M. Provencio, New molecular targeted therapies for advanced non-small-cell lung cancer, *J. Thorac. Dis.*, 2011, **3,** 30-56.

[5] P.L. Paris, Y. Kobayashi, Q. Zhao, W. Zeng, S. Sridharan, T. Fan et al., Functional phenotyping and genotyping of circulating tumor cells from patients with castration resistant prostate cancer. *Cancer Lett.*, 2009, 227, **2,** 164-173.

[6] M. Pestrin, S. Bessi, F. Galardi, M. Truglia, A. Biggeri, C. Biagioni et al., Correlation of HER2 status between primary tumors and corresponding circulating tumor cells in advanced breast cancer patients, *Breast Cancer Res. Treat.*, 2009, 118, **3,** 523-530.

[7] N. Xenidis, M. Ignatiadis, S. Apostolaki, M. Perraki, K. Kalbakis, S. Agelaki et al., Cytokeratin-19 mRNA-positive circulating tumor cells after adjuvant chemotherapy in patients with early breast cancer. *J. Clin. Oncol.*, 2009, 27, **13,** 2177-2184.

[8] A. Marusyk, V. Almendro and K. Polyak, Intra-tumour heterogeneity: a looking glass for cancer. *Nature Reviews Cancer*, 2012, **12,** 323-334.

[9] A. A. Powell, A. A. H. Talasaz, H. Zhang, M. A. Coram, A. Reddy, G. Deng, M. L. Telli et al., Single Cell Profiling of Circulating Tumor Cells: Transcriptional Heterogeneity and Diversity from Breast Cancer Cell Lines, *PlosONE*, 2012, 7, **5,** e33788.

[10] M. Labelle and R. O. Hynes, The initial hours of metastasis: The importance of cooperative host-tumor cell interactions during hematogenous dissemination, *Cancer Discovery*, 2012, **2,** 1091-1099.

[11] T. R. Ashworth, A case of cancer in which cells similar to those in the tumours were seen in the blood after death, *The Medical Journal of Australia*, 1869, **14,** 146-147.

[12] M. Cristofanilli, K. R. Broglio, V. Guarneri, S. Jackson, H.A. Fritsche, R. Islam et al., Circulating tumor cells in metastatic breast cancer: biologic staging beyond tumor burden, *Clin. Breast Cancer*, 2007, 7, **6,** 471-479.

[13] J. S. de Bono, H. I. Scher, R. B. Montgomery, C. Parker, M. C. Miller, H. Tissing et al., Circulating tumor cells predict survival benefit from treatment in metastatic castration-resistant prostate cancer, *Clin. Cancer Res.*, 2008, **14,** 6302-6309.

[14] G. T. Budd, M. Cristofanilli, M. Ellis, et al., Circulating tumor cells versus imaging - predicting overall survival in metastatic breast cancer, *Clin Cancer Res*, 2006, 12, **21,** 6403-6409.

[15] V. Gupta, I. Jafferji, M. Garza, V. O. Melnikova, D. K. Hasegawa et al., ApoStream™, a new dielectrophoretic device for antibody independent isolation and recovery of viable cancer cells from blood, *Biomicrofluidics*, 2012, **6,** 024133.

[16] P. Augustsson et al., Microfluidic, label-free enrichment of prostate cancer cells in blood based on acoustophoresis, *Anal. Chem.*, 2012, 84, **18,** 7954-7962.

[17] Thege FI, Lannin TB, Saha TN, Tsai S, Kochman ML, Hollingsworth M a, et al. Microfluidic immunocapture of circulating pancreatic cells using parallel EpCAM and MUC1 capture: characterization, optimization and downstream analysis. *Lab Chip*. 2014;14:1775–84.

[18] Riethdorf S, Fritsche H, Müller V, Rau T, Schindlbeck C, Rack B, et al. Detection of circulating tumor cells in peripheral blood of patients with metastatic breast cancer: a validation study of the CellSearch system. *Clin Cancer Res*. 2007;13:920–8.

[19] Miller MC, Doyle G V, Terstappen LWMM. Significance of Circulating Tumor Cells Detected by the CellSearch System in Patients with Metastatic Breast Colorectal and Prostate *Cancer*. *J Oncol*. 2010;2010:617421.

[20] Yang J, Weinberg R a. Epithelial-mesenchymal transition: at the crossroads of development and tumor metastasis. *Dev Cell*. 2008;14:818–29.

[21] Bonnomet A, Brysse A, Tachsidis A, Waltham M, Thompson EW, Polette M, et al. Epithelial-to-mesenchymal transitions and circulating tumor cells. *J Mammary Gland Biol Neoplasia*. 2010;15:261–73.

[22] A. Williams, M. Balic, R. Datar and R. Cote, Size-Based Enrichment Technologies for CTC Detection and Characterization, *Recent Results in Cancer Research*, 2012, **195,** 87-95.

[23] G. Vona, A. Sabile, M. Louha, V. Sitruk, S. Romana, K. Schutze, F. Capron, D. Franco, M. Pazzagli et al., Isolation by Size of Epithelial Tumor Cells: A New Method for the Immunomorphological and Molecular Characterization of Circulating Tumor Cells, *The American Journal of Pathology*, 2000, **156,** 1, 57-63.

[24] H. K. Lin, S. Zheng, A. J. Williams, M. Balic, S. Groshen, H. I. Scher et al., Portable Filter-Based Microdevice for Detection and Characterization of Circulating Tumor Cells, *Clin. Cancer Res*., 2010, 16, **20,** 5011-5018.

[25] S. Zheng et al., Membrane microfilter device for selective capture, electrolysis and genomic analysis of human circulating tumor cells. *J. Chromatogr. A*, 2007, 1162, **2,** 154-61.

[26] I. Desitter, B. S. Guerrouaheni, N. Benali-Furet, J. Wechsler, P. A. Janne, Y. Kuang et al., A new device for rapid isolation by size and characterization of rare circulating tumor cells. *Anti-Cancer Research*, 2011, **31,** 427-442.

[27] V. De Giorgi, P. Pinzani, F. Salvianti, J. Panelos, M. Paglierani, A. Janowska, M. Grazzini et al., Application of a Filtration- and Isolation-by-Size Technique for the Detection of Circulating Tumor Cells in Cutaneous Melanoma, *Journal of Investigative Dermatology*, 2010, **130,** 2440-2447.

[28] J. M. Hou et al., Circulating Tumor Cells as a Window on Metastasis Biology in Lung Cancer, *Am. J. Pathol.*, 2011, 178, **3,** 989-996.

[29] Jin C, McFaul SM, Duffy SP, Deng X, Tavassoli P, Black PC, et al. Technologies for label-free separation of circulating tumor cells: from historical foundations to recent developments. *Lab Chip*. 2013;14:32–44.

[30] Harouaka R a., Nisic M, Zheng S-Y. Circulating Tumor Cell Enrichment Based on Physical Properties. *J Lab Autom*. 2013;18:455–68.

[31] Zhou M-D, Hao S, Williams AJ, Harouaka R a., Schrand B, Rawal S, et al. Separable Bilayer Microfiltration Device for Viable Label-free Enrichment of Circulating Tumour Cells. *Sci Rep*. 2014;4:7392.

[32] Lin BK, McFaul SM, Jin C, Black PC, Ma H. Highly selective biomechanical separation of cancer cells from leukocytes using microfluidic ratchets and hydrodynamic concentrator. *Biomicrofluidics*. 2013;7:034114.

[33] Lee A, Park J, Lim M, Sunkara V, Kim SY, Kim GH, et al. All-in-One Centrifugal Microfluidic Device for Size-Selective Circulating Tumor Cell Isolation with High Purity. *Anal Chem*. 2014;86:11349–56.

[34] Harouaka R a., Zhou M Da, Yeh YT, Khan WJ, Das A, Liu X, et al. Flexible micro spring array device for high-throughput enrichment of viable circulating tumor cells. *Clin Chem*. 2014;60:323–33.

[35] Lin HK, Zheng S, Williams AJ, Balic M, Groshen S, Scher HI, et al. Portable filter-based microdevice for detection and characterization of circulating tumor cells. *Clin Cancer Res*. 2010;16:5011–8.

[36] Zheng S, Lin HK, Lu B, Williams A, Datar R, et al. 3D microfilter device for viable circulating tumor cell (CTC) enrichment from blood. *Biomed Microdevices*. 2011;13:203–13.

[37] J. den Toonder, Circulating tumor cells: the Grand Challenge, *Lab Chip*, 2011, **11,** 375-377.

[38] Yamada M, Seki M. Hydrodynamic filtration for on-chip particle concentration and classification utilizing microfluidics. *Lab Chip*. 2005;5:1233–9.

[39] Shen S, Ma C, Zhao L, Wang Y, Wang J-C, et al. High-throughput rare cell separation from blood samples using steric hindrance and inertial microfluidics. *Lab Chip*. 2014;14:2525–38.

[40] Liu Z, Huang F, Du J, Shu W, Feng H, Xu X, et al. Rapid isolation of cancer cells using microfluidic deterministic lateral displacement structure. *Biomicrofluidics*. 2013;7.

[41] Loutherback K, D'Silva J, Liu L, Wu A, Austin RH, Sturm JC. Deterministic separation of cancer cells from blood at 10 mL/min. *AIP Adv*. 2012;2:1–8.

[42] Di Carlo D. Inertial microfluidics. *Lab Chip*. 2009;9:3038–46.

[43] Martel JM, Toner M. Inertial focusing in microfluidics. *Annu Rev Biomed Eng*. 2014;16:371–96.

[44] Zhou J, Papautsky I. Fundamentals of inertial focusing in microchannels. *Lab Chip*. 2013;13:1121–32.

[45] Shin JH, Lee MG, Choi S, Park J-K. Inertia-activated cell sorting of immune-specifically labeled cells in a microfluidic device. *RSC Adv*. 2014;4:39140.

[46] Lee MG, Shin JH, Bae CY, Choi S, Park J. Label-Free Cancer Cell Separation from Human Whole Blood Using Inertial Microfluidics at Low Shear Stress. *Anal Chem*. 2013;85:6213–8.

[47] Bhagat AAS, Hou HW, Li LD, Lim CT, Han J. Pinched flow coupled shear-modulated inertial microfluidics for high-throughput rare blood cell separation. *Lab Chip*. 2011;11:1870–8

[48] Hou HW, Warkiani ME, Khoo BL, Li ZR, Soo R a, Tan DS-W, et al. Isolation and retrieval of circulating tumor cells using centrifugal forces. *Sci Rep*. 2013;3:1259.

[49] Warkiani ME, Guan G, Luan KB, Lee WC, Bhagat AAS, Kant Chaudhuri P, et al. Slanted spiral microfluidics for the ultra-fast, label-free isolation of circulating tumor cells. *Lab Chip*. 2013;14:128–37.

[50] Khoo BL, Warkiani ME, Tan DSW, Bhagat AAS, Irwin D, Lau DP, et al. Clinical validation of an ultra high-throughput spiral microfluidics for the detection and enrichment of viable circulating tumor cells. *PLoS One*. 2014;9:1–7.

[51] Ozkumur E, Shah AM, Ciciliano JC, Emmink BL, Miyamoto DT, Brachtel E, et al. Inertial focusing for tumor antigen-dependent and -independent sorting of rare circulating tumor cells. *Sci Transl Med*. 2013;5:179ra47.

[52] G. Segre and A. Silberberg, Radial Particle Displacements in Poiseuille Flow of Suspensions, *Nature*, 1961, **189,** 209-210.

[53] D. Di Carlo, Inertial Microfluidics, *Lab Chip*, 2009, **9,** 3038-3046.

[54] A. A. S. Bhagat et al., Inertial Microfluidics for Continuous Particle Filtration and Extraction, *Microfluid. Nanofluid.*, 2008, **7,** 217-226.

[55] H. Moffatt, *J. Fluid Mech.*, 1964, 18, **1,** 1-18.

[56] W. Cherdron, F. Durst, and J. Whitelaw, *J. Fluid Mech.*, 1978, 84, **13**.

[57] Friend J, Yeo L. Fabrication of microfluidic devices using polydimethylsiloxane. *Biomicrofluidics*. 2010;4:026502.

[58] A. J. Mach, J. H. Kim, A. Arshi, S. C. Hur & D. Di Carlo. Automated cellular sample preparation using a Centrifuge-on-a-chip. *Lab Chip*, 2011, **11,** 2827-2834.

[59] S. Nagrath, L. V. Sequist, S. Maheswaran, D. W. Bell, D. Irimia, L. Ulkus, M. R. Smith, E. L. Kwak, S. Digumarthy, A. Muzikansky, P. Ryan, U. J. Balis, R. G. Tompkins, D. A. Haber & M. Toner, Isolation of rare circulating tumor cells in cancer patients by microchip technology, *Nature*, 2007, **450,** 1235-1239.

[60] R. Strauss, Z. Y. Li, Y. Liu, I. Beyer, J. Persson, P. Sova, T. Möller, S. Pesonen, A. Hemminki, P. Hamerlik, C. Drescher, N. Urban, J. Bartek, A. Lieber, Analysis of epithelial and mesenchymal markers in ovarian cancer reveals phenotype heterogeneity and plasticity, *PlosONE*, 2011, 6, **1,** e16186.

[61] Y. Kim, H.S. Kim, Z.Y. Cui, H.S. Lee, J.S. Ahn, C.K. Park, K. Park, M.J. Ahn, Clinicopathological Implications of EpCAM Expression in Adenocarcinoma of the Lung, *Anticancer Research*, 2009, 29, **5,** 1817-1822.

[62] S. C. Hur, N.K. Henderson-MacLennan, E. R. B. McCabe, and D. Di Carlo, Deformability-Based Cell Classification and Enrichment Using Inertial Microfluidics, *Lab Chip*, 2011, **11,** 912-920.

[63] D. R. Gossett, H. T. K. Tse, S. A. Lee, Y. Ying, A. G. Lindgren, O. O. Yang, J. Rao, A. T. Clarck, D. Di Carlo. Hydrodynamic stretching of single cells for large population mechanical phenotyping, *PNAS*, 2012, 109, **20,** 7630-7635.

Chapter 2: Purification of Pleural Effusions for Cytodiagnostics

Vortex technology was first clinically applied to isolate DTCs in pleural effusions. The following chapter highlights the automatability of Vortex technology and its use as a sample preparation tool for purifying DTCs to facilitate ease of diagnostics in cytopathology.

Current methods and limitations in cytopathology

The pleural space surrounds the lungs and is lined by the pleural sac. Under certain conditions, including malignancies, this space can fill with excess fluid, resulting in a pleural effusion, which is often removed in a procedure termed thoracentesis for diagnostic and therapeutic purposes. Over 1.5 million thoracentesis procedures are conducted annually in the United States [1]. Many cell types may be present within the pleural effusion, and isolating these cells is important to identify the ongoing disease process. Cytologists analyze pleural samples to determine the cause (presence or absence of cancer) by examining stained cell smears on a glass slide. Sample preparation and analysis requires technician-intensive sample handling involving multiple centrifugation steps followed by staining and time-consuming manual microscopic scanning of cytology slides by the cytopathologist, who must search for key cancer cell morphological characteristics, such as high nuclear-to-cytoplasmic ratios, hypochromatic cytoplasms, and dense, dark nuclei.

DTCs originating from the lung, breast, or other organs can be identified in malignant pleural effusions. Traditional cytomorphological analysis of cell smears and blocks has high specificity, but low sensitivity. The low sensitivity can be either due to the subjective nature of analysis, loss of tumor cells during processing, or the fact that there may be few tumor cells present in a large specimen volume. Moreover, pleural fluids from cancer patients are diverse in cellularity and consistency, ranging from a trasparent yellow to bloody and opaque (Fig. 1.1B).

As a result, traditional cytological examinations may fail to identify malignant cells in up to 40% of cases [2]. Therefore, approaches to obtaining these malignant cells from larger volumes of fluid with high purity and efficiency could improve cytology-based diagnoses [3]. Additional applications for purified cells from pleural and other body fluids include the ability to probe cellular properties such as cell deformability [4,5], evaluation of effusion microenvironments [6], and identifying cellular metastases [7].

Increasing sample purity enables improved molecular diagnostics to detect the presence of specific genetic mutations which may be amenable to targeted therapies. This can be achieved by removing a large population of leukocytes that contain interfering wild-type DNA. For genetic testing such as quantitative PCR (qPCR), the presence of a small quantity of mutated genes can be overshadowed by a large background of wild type nucleic acids. Using qPCR, the cycle threshold (Ct) gives a relative measurement of the amount of genetic material of interest that is present; a lower Ct indicates a greater amount of the gene of interest. Although qPCR can be exquisitely sensitive for mutation detection given appropriate selection of amplification primers, there is often some non-specific amplification from background DNA. The presence of large quantities of background DNA can thus interfere with accurate measurement of the Ct due to this non-specific amplification; this effect may still be notable even after normalization with housekeeping genes.

There are several approaches that are currently utilized to isolate cells of interest from pleural effusions for molecular analysis. The gold standard is laser capture microdissection (LCM), a technique used to isolate pure populations from cytology fluids, live cell culture, or heterogeneous tissue sections [8-12]. However, this technique requires drying out of cells during capture, which can lead to cell damage and is not capable of extracting large quantities of cells

for analysis. It is also very time consuming and labor intensive. Flow cytometry and fluorescence activated cell sorting (FACS) are also common methods for cell separation and sorting. While FACS can process samples of up to 30 mL in 1 hr, the sorted cells may not be suitable for further analysis as a result of the initial fixing and cell type-specific staining required for the sorting process. Alternatively, several microfluidic strategies have been used to isolate and enrich tumor cells in body fluid [13], such as the use of self-assembled magnetic beads coated with anti-CD19 antibodies to capture B-cell malignant tumors [14]. However, current technologies are limited by throughput and purity, and none have been placed in widespread use in clinical labs for a variety of reasons. Many devices also focus on rare cell isolation from blood, as highlighted in Chapter 1, rather than tumor cell enrichment from pleural effusions, which have unique fluid properties and cellular profiles. Ideally, rapid sampling of pleural fluids (often liters of fluid) requires mL/min processing rates and separation using a label-free marker such as cell size [15]. Moreover, sample preparation of pleural effusions should be performed in an automated, repeatable fashion to enable clinicians and cytopathologists to perform molecular assays on the purified cells with the highest possible sensitivity and specificity in a short time period (tens of minutes).

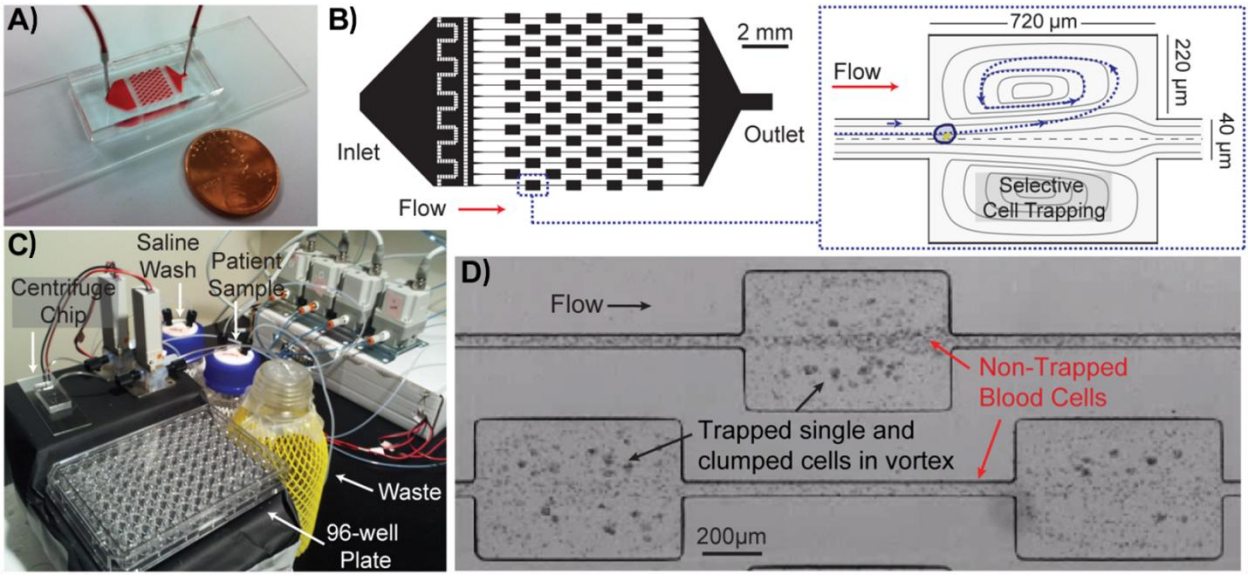

Figure 2.1: Principles of the Centrifuge Chip. (A) A photograph of the Centrifuge Chip device. Only a single inlet and outlet is required. **(B)** A schematic of the massively parallel microfluidic device that selectively traps large cells in individual microscale vortices. **(C)** A photograph of the device connected to an automated fluidic instrument to deliver patient pleural samples and saline wash through the Centrifuge Chip into the waste bottle or collection plate. Trapped epithelial and mesothelial cells are made readily available i) into a collection tube for further cytology slide comparisons with the original and/or ii) into a well-plate for immunolabeling, imaging and analysis. **(D)** High-speed microscopic image showing trapping of larger single and clumped cells while smaller red and white blood cells pass through.

Adjustment of Vortex technology for pleural effusions

A Vortex design known as the Centrifuge Chip was previously demonstrated to recapitulate the high-throughput enrichment and concentration operations of a standard laboratory centrifuge [16], and was implemented for clinical applications with pleural effusions. Here, the Centrifuge Chip was modified (Fig. 2.1) to include: i) integration with a custom-made pressure system that operates using a simple ‘plug-and-play’ option in which an operator does not need to be present at all times, ii) shortened device channel length to reduce fluidic resistance, and iii) increased number of parallel channels to 16 with 8 chambers in each channel for a total of 128 cell trapping reservoirs to process samples at an optimal flow rate of 6 mL/min. At this flow rate one patient sample (~50 ml of volume) requires <10 minutes to process. The

capture efficiency of the device was ~47%, which was defined as the number of 20 μm diameter beads caught and released from the vortices divided by the total number of beads injected.

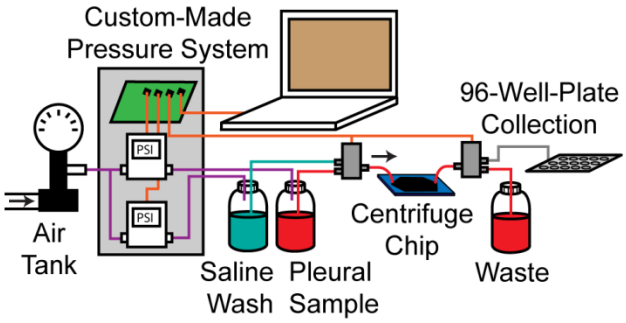

Centrifuge Chip Operations	Saline Wash	Pleural Sample	Waste	Collection
Processing	Off	On	On	Off
Washing	On	Off	On	Off
Release	On	Off	Off	On

Figure 2.2: Centrifuge Chip system schematic and operations. Sample processing is controlled using an automated pressure system comprised of an air tank, pressure regulators, air and liquid valves, and a computer with a LabVIEW (National Instruments) user interface. A liquid valve upstream from the device switches between the saline wash and pleural sample bottles, and the downstream valve directs fluid between the waste and collection containers. The procedure involves three key steps, including: i) processing the fluid sample to capture potential cancer cells, ii) washing the device reservoirs to remove smaller leukocytes and RBCs while maintaining the same flow rate and active microvortices to keep larger cells trapped, and iii) lowering the flow rate to release the captured cells from the vortices and into a 96-well plate.

The disposable device is connected to an automated custom-made pressure system that delivers effusion samples or saline wash from pressurized glass bottles through the Centrifuge Chip (Fig. 2.1C). The LabVIEW-controlled system contains a pair of air regulators, air valves and liquid valves (SMC Corporation) that brings compressed air into the bottles and drives fluid through the microchip device (Fig. 2.2). Non-diluted pleural effusion samples are poured directly into the glass bottle and introduced through the device at 6 mL/min. Once the vortex traps are filled with cells, PBS is introduced into the device to wash out untrapped blood cells in the main flow and the vortex traps. Cells trapped in the fluid vortex are released by reducing the input air pressure and subsequently lowering the flow rate and dissipating the vortex. A ‘trap-and-release’

program was implemented to continuously introduce sample through the Centrifuge Chip, wash, and release the captured cells in a small 250 μL volume into a microtiter plate or collection vial.

Enriched cell size distributions in pleural effusions

Remnants of 115 pleural effusion samples obtained from Ronald Reagan UCLA Medical Center, Santa Monica UCLA Medical Center, and Northridge Hospital Medical Center were used in the study. From all specimens, up to 50 mL of sample were processed with the Centrifuge Chip. Effusions were passed through a 40 μm cell strainer before introducing through the Centrifuge Chip system. Measurements were conducted on the number and diameter of cells present in 25 pleural fluid samples (Fig. 2.3). Dilute volumes of unprocessed and processed pleural samples were lysed with red blood cell lysis buffer (Roche) and incubated with Calcein AM (Invitrogen) for 15 minutes. Cells were imaged using a Nikon Eclipse Ti fluorescent microscope, and cell sizes were automatically measured using Nikon NIS-Elements AR 3.2 software.

A population of cells greater than 15 μm was observed in malignant samples (Fig. 2.3A**)**, consistent with the observation that malignant and mesothelial cells are usually larger compared to other cells present within these fluids [17]. Cases of inflammation had a large population of 10-15 μm cells, potentially representing the characteristic population of large activated immune cells. Of the samples diagnosed as positive for malignancy, on average 36.57% of nucleated cells were larger than 15 μm. A lower percentage of larger cells was present in samples diagnosed as negative and negative with inflammation (32.47% and 26.92% of nucleated cells larger than 15 μm, respectively). Cases with inflammation are known to have a larger number of white blood cells as a fraction of the population, thus leading to a lower relative percentage of larger cells than negative samples alone. Note that these relatively large percentages of larger cells in non-

malignant samples are likely the result of the presence of mesothelial cells and large activated leukocytes. Still, malignant samples contain the largest fraction of large cells such that cell size is a potential biomarker for harvesting malignant cells from pleural fluid samples. The Centrifuge Chip enriched for the cell populations greater than 15 µm (Fig. 2.3B).

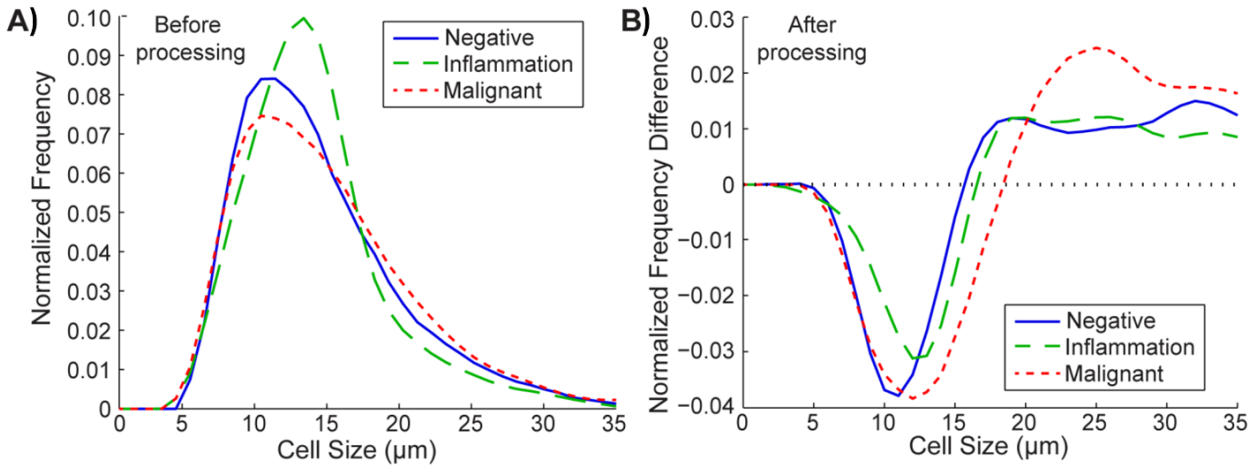

Figure 2.3: Size distributions of enriched cells from pleural fluids. **(A)** Normalized frequency distributions of nucleated cells in relation to cell diameter are plotted for pleural effusions analyzed within 24 hours of collection and diagnosed as negative (blue, solid), inflammation (chronic and acute, green, dashed), or malignant (red, dotted). Relative to negative pleural effusions, malignant samples contain a larger population fraction of cells greater than 15 µm, and cases of inflammation contain a larger population of cells between 10-15 µm. N = 13, 9, and 10 for negative, inflammation, and malignant cases. **(B)** The frequency distributions of the same samples after processing through the Centrifuge Chip were subtracted by the distributions before processing to observe enrichment. The device enriches for cell populations greater than 15 µm and depletes smaller cells.

Increased sample purity through the Centrifuge Chip for cytology

Half of the processed samples were returned to the cytology laboratory to create cell smears. This was performed in parallel with cell smears produced with traditional cytological methods on original, unprocessed samples. The other half of processed samples were fluorescently labeled to quantify sample purity (Fig. 2.4). A fraction of samples were profiled for cell size distributions before and after processing. Smears were prepared according to normal methods to prepare samples for clinical evaluation. Briefly, samples were aliquoted into 50 mL

conical tubes and centrifuged down with a standard benchtop centrifuge. After centrifugation, the supernatant is aspirated and the cells are resuspended in a buffer solution and placed with a glass slide into a cytocentrifuge (Thermo Scientific) to create a cell smear. The cell slides are air dried or fixed and stained with Papanicolou (Pap) or May-Grunwald-Giemsa (MGG) stains.

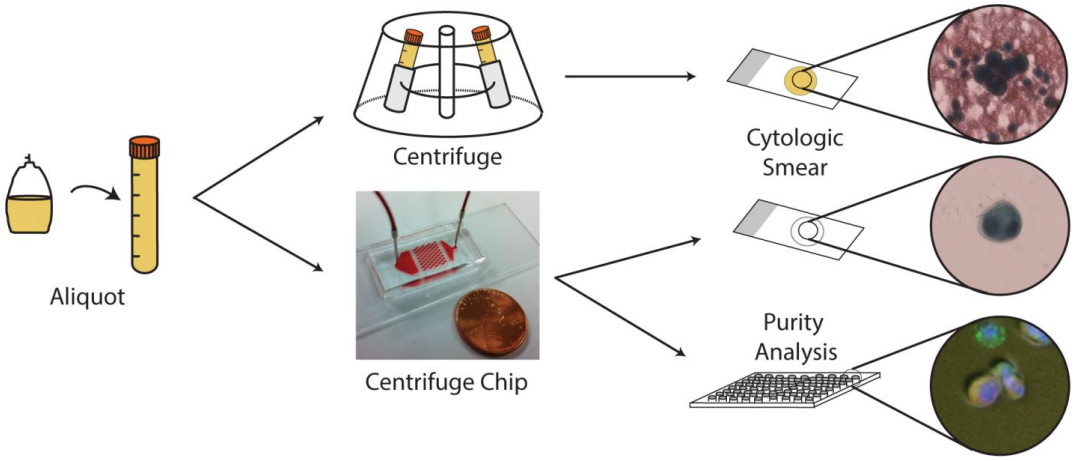

Figure 2.4: Sample processing flow with the Centrifuge Chip. 50 mL of pleural effusion sample were processed using traditional cytological methods and the Centrifuge Chip. A portion of cells harvested from the Centrifuge Chip was returned to the cytopathology laboratory to create cell smears; the other portion of processed sample was immunolabeled for purity analysis.

In all samples, malignant and mesothelial cells are found amongst a cellular background of red and white blood cells in standard cytology slides while there are few background cells observed in the Centrifuge Chip-prepared sample slides (Figs. 2.5A-F). Malignant cells are characterized by large nuclei and high nuclear-cytoplasmic ratios, and are often seen as cell aggregates or clumps in effusions [1], which are also found from the Centrifuge Chip. The Centrifuge Chip may aid pathologists in rapid visualization of rarer malignant cells which may improve diagnostic sensitivity especially by enabling processing of larger volumes of fluid into a minimal final concentrated sample volume.

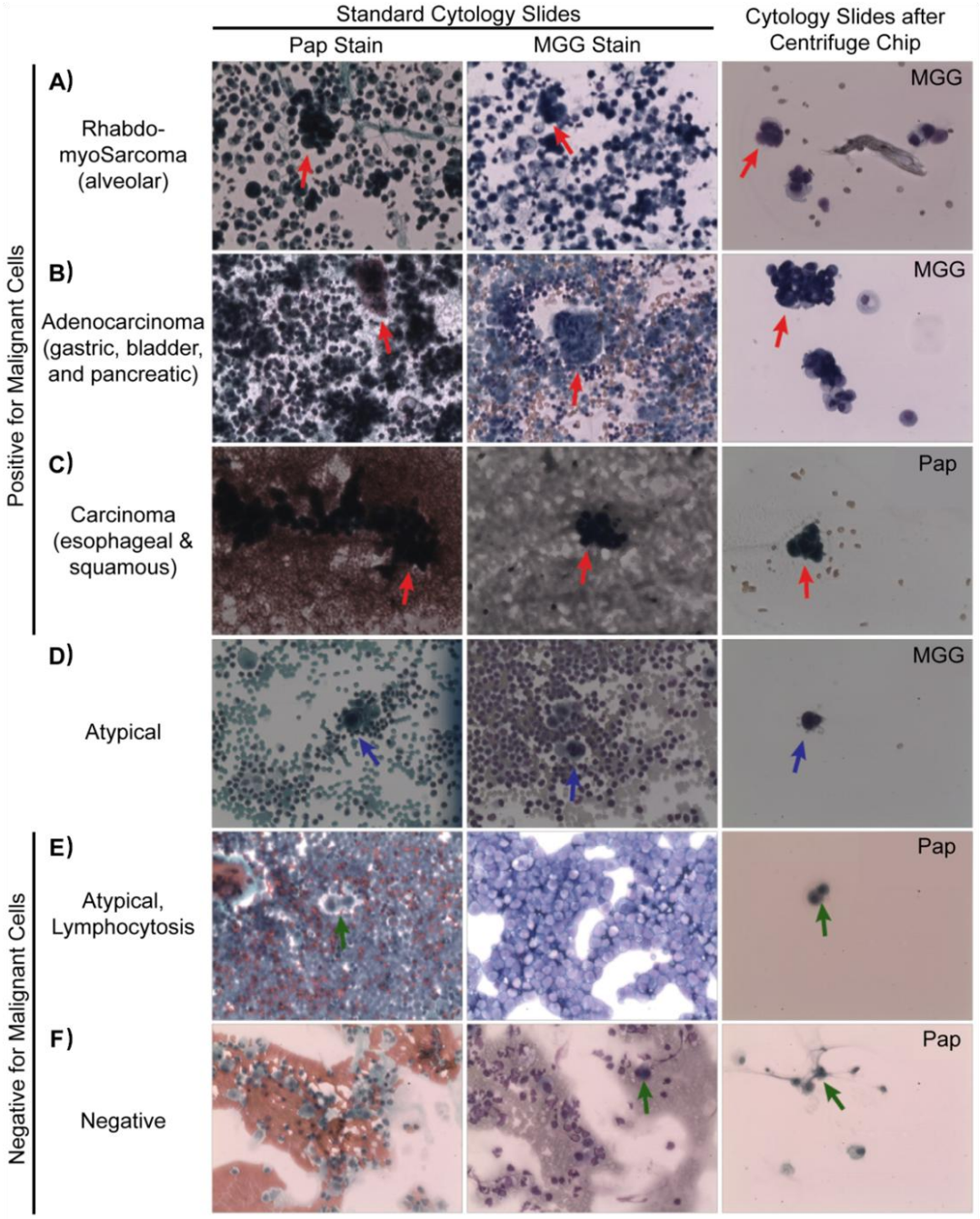

Figure 2.5: Reduced background in cytology slides. Unprocessed and processed patient samples were prepared with Pap and MGG stains. In all samples, malignant and mesothelial cells are found amongst a cellular background of immune cells in standard slides while little background is observed in the Centrifuge Chip slide. In samples diagnosed as 'positive for malignancy', single and clumped malignant cells (red arrows) are retrieved following the Centrifuge Chip. In patients diagnosed as 'negative for malignancy', mesothelial cells (green arrows) were found amongst a background of blood cells in standard slides, compared to no blood cell background upon Centrifuge Chip Processing. Samples diagnosed as atypical contained cells which resembled either malignant or mesothelial cells (blue arrows). Images obtained at 200x magnification.

To better quantify the enrichment of processed samples, immunofluorescent staining was performed on the processed sample and original sample. Up to 10 mL effusion volume was processed with the Centrifuge Chip and isolated cells were released in a volume of ~250 μL in the microtiter plate. Cells were fixed and permeabilized as described previously (Chapter 1, p. 9), and stained CK-PE, CD45-FITC, and DAPI in 2% w/v BSA. After staining, cells were imaged using a CCD camera (Photometrics CoolSNAP HQ2) mounted on a Nikon Eclipse Ti microscope. The whole well was automatically imaged in a few minutes (100X) using an ASI motorized stage operated with Nikon NIS-Elements AR 3.2 software. Captured images were automatically obtained for four configurations: brightfield, FITC, TRITC and DAPI filter sets. Collected images were automatically stitched together using the NIS-Elements Software. Images were analyzed by enumerating the number of CK+ and CD45+ cells present in each well. CK+ cells include both carcinoma cells and mesothelial cells. No attempts were made to separate tumor cells from mesothelial cells as these cells share a similar size, but these separations can be carried out using IHC markers such as Calretinin [21], if necessary, to further enrich a specimen.

The device increased purity in all 66 cases examined (100%) (Fig. 2.6). Paired t-tests between unprocessed and processed samples demonstrated a significant increase in purity, with p values less than 0.05 for all diagnoses. In agreement with cell size measurements, many cells were captured for malignancy-positive cases and fewer for malignancy-negative cases with lymphocytosis, reactive changes, or acute inflammation. Greater than 65-fold enrichment was observed for samples diagnosed as positive for malignancy. Interestingly, samples with chronic inflammation had a 132-fold increase as a result of the larger leukocyte populations in the initial samples with <1% purity.

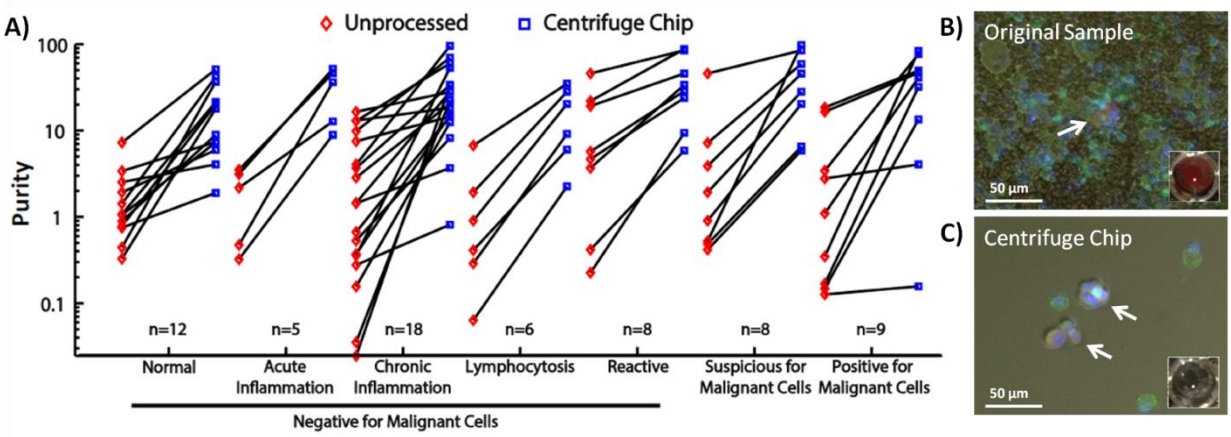

Figure 2.6: Increased purity from paired samples following Vortex processing. (A) The purity of epithelial and mesothelial cells in all samples (n = 66) increases upon processing with the Centrifuge Chip. **(B, C)** Qualitative comparison of unprocessed and processed samples reveal significant reduction in contaminating background cells with the Centrifuge Chip. Immunofluorescent images show CK (red – epithelial cells), CD45 (green – leukocytes), and DAPI (blue – nucleus). Insets show well-plate color: red (indicating bloody) and colorless (after processing with device). Arrows indicate CK+/DAPI+ epithelial cells.

High sensitivity of detection of point mutations

The Centrifuge Chip was also assessed for its ability to improve the accuracy of mutational analysis by analyzing spiked pleural effusions before and after enrichment. Initial cell concentration was quantified using a hemacytometer after performing a red blood cell lysis step. A549 lung cancer cells (ATCC) were spiked at 0.1% purity in 50 mL of pleural effusions diagnosed as negative for malignancy. Spiked samples were evaluated for the A549 34 G>A substitution in KRAS (KRAS*) as identified by the Sanger Cosmic database [18]. Quantitative reverse transcriptase polymerase chain reaction (qRT-PCR) was employed to identify mutant KRAS in the A549 cells versus wild type (in HeLa and other cells) using a modification of the system described by Morlan et al. (2009) [19]. The amplification required a primer complementary to the mutant and a blocking primer with a non-hydrolyzable phosphate group complementary to the wild type sequence which was present at four times the concentration. The rationale for this strategy was that the non-hydrolyzable primer would block non-specific

amplification from the wild type sequence while still allowing amplification from the mutant of interest. GAPDH mRNA was also amplified as an indicator for the relative number of cells in a given sample and used to normalize each measurement to determine the ΔCt value.

Briefly, reverse transcription was performed using a SuperScript III RT kit (Invitrogen) according to the manufacturer's instructions to create cDNA libraries. TaqMan PCR was performed using 2 µL of the RT product in a 20 µL total volume with 1x TaqMan Universal PCR Master Mix (no UNG) (Roche) with the primers at 900 nM, TaqMan probe at 200 nM, and blocker at 3600 nM. Stock TaqMan probes for GAPDH and KRAS were obtained from Applied Biosystems and used without modification. The thermocycling conditions were as follows: 10 minutes at 95°C, 40 cycles of 20 seconds at 95°C and 1 minute at 60°C.

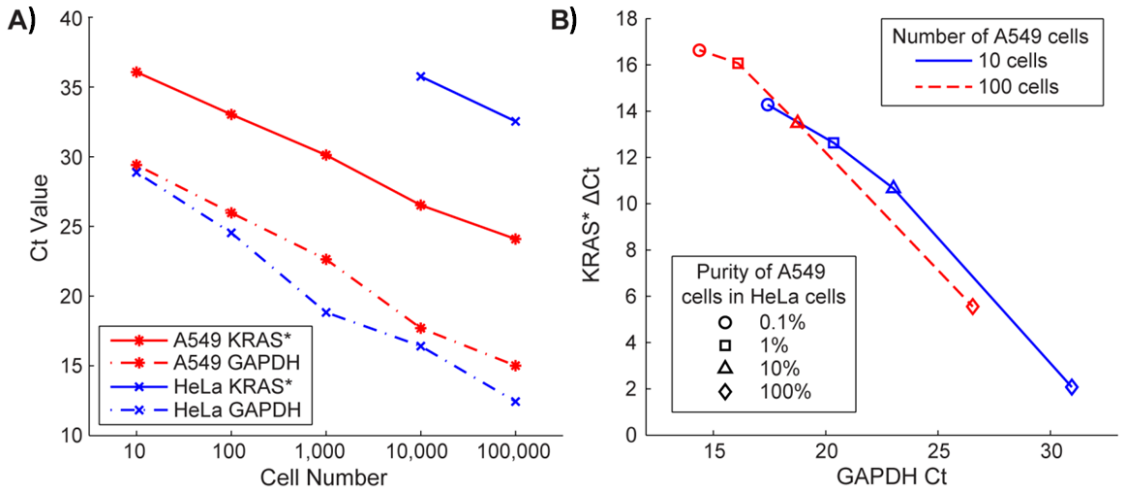

Figure 2.7: Effect of cell number and purity on PCR. (A) Quantitative RT-PCR was performed on cell lines with varying cell number. Ct values for KRAS* (solid line) and GAPDH (dotted line) decreased with increasing cell number. KRAS* Ct for samples with 1,000 HeLa cells or fewer was not detected. **(B)** KRAS* ΔCt decreases with increasing purity of A549 cells spiked in a larger population of HeLa cells.

Non-specific amplification from background cells can reduce confidence when measuring the presence of mutations. Pure populations of 10^5 A549 cells which contain the KRAS* mutation and HeLa cells which have wild type KRAS were measured to have threshold cycles (Ct) of 24.10 and 32.53 respectively (the latter value indicating nonspecific amplification

for wild type KRAS from HeLa cells). In mixed samples of A549 and HeLa, the presence of the specific KRAS mutation could be distinguished from background at as low as 0.1% purity of A549 cells, with as few as 10 A549 cells present (Fig. 2.7). Note that the same Ct values can be observed from low numbers of A549 cells with specific amplification occurring, or large numbers of HeLa cells with non-specific amplification (see 10,000 HeLa cells vs. 10 A549 cells, Fig. 2.7A). Therefore, data was normalized to account for cell number by subtracting GAPDH Ct from KRAS Ct values, yielding a KRAS* ΔCt. As expected, increased purity samples yielded improved results, characterized by a lower ΔCt (Fig. 2.7B).

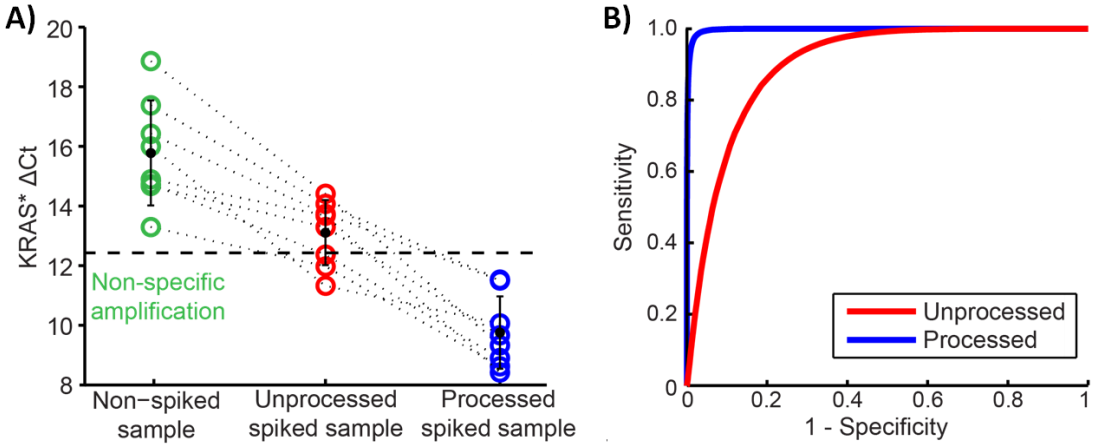

Figure 2.8: Enhanced RT-PCR detection confidence. (A) RT-PCR was performed on non-spiked, unprocessed spiked samples (0.1% purity), and processed spiked samples. KRAS* ΔCt decreased in all cases (n=7), demonstrating an improved signal for the KRAS mutation. Compared to non-spiked samples, processed spiked samples exhibit a clearer KRAS* ΔCt which is more distinct than for unprocessed spiked samples. The dotted black line shows a 12.2 Ct cut-off threshold for the KRAS mutation. **(B)** Receiver operating characteristic curves are plotted based on a Gaussian distribution of samples shown in part A. Processed samples show higher area under curve (AUC) values at 0.998 (blue, solid), compared with 0.905 (red, dashed) for unprocessed samples.

The Centrifuge Chip also improved the sensitivity and specificity in detecting A549 cells spiked into negative clinical effusion samples at 0.1% purity (Fig. 2.8). Non-spiked negative samples (including acute and chronic inflammation samples) averaged a KRAS* ΔCt of 15.7 ± 1.76 (N=7), and spiked samples at 0.1% purity averaged 12.8 ± 1.39. Once processed with the

Centrifuge Chip, the KRAS* ΔCt decreased and became further differentiated from the negative samples in all cases (Fig. 2.8A) with an average of 9.6 ± 1.19 ΔCt. Average GAPDH Ct values were 17.63 ± 2.10, 17.80 ± 2.05, and 23.75 ± 2.03 for negative samples, unprocessed spiked samples, and processed spiked samples, respectively. A paired t-test between non-spiked and spiked samples demonstrated improved statistical significance in the difference in the average KRAS* ΔCt after spiked samples were processed with the Centrifuge Chip ($p = 0.0027$ before and $p = 1.44e\text{-}6$ after processing). Moreover, using a Gaussian distribution fit to ΔCt values for each group of samples, receiver operating characteristic curves (Fig. 2.8B) demonstrated improved area under curve (AUC) values from 0.905 (unprocessed spiked samples) to 0.998 (processed spiked samples). The upper cutoff threshold for a positive KRAS* ΔCt diagnosis was determined by maximizing both sensitivity and specificity, and it was found to be 14.1 for unprocessed and 12.2 for processed samples. By increasing sample purity with the device, improvements are made toward KRAS mutation detection and diagnostic confidence.

For a highly specific assay like PCR, the simple concentration and enrichment approach has the potential to improve diagnostic accuracy for mutational detection when the original mutation is known (e.g., in a sequenced tumor). The technique is expected to be particularly useful in less specific assays, such as gene sequencing, if a particular gene mutation is suspected but the source unknown. As next generation sequencing technologies improve, it may even be possible to do whole transcriptome sequencing, and achieving high purity using an approach such as this would be essential to detect mutations of interest while suppressing non-specific wild-type reads.

Concluding remarks

By processing a large volume of fluid and selectively enriching larger cells over a background of red and white blood cells, the Centrifuge Chip replaces the traditional centrifugation step in the clinical lab while also potentially enabling more sensitive analysis of purer preparations originating from large volume samples. The device rapidly isolates larger and potentially malignant cells from pleural effusions in a label-free manner with high purity, and resolves issues of reducing background cell populations and limiting the area of microscopic evaluation in cytology slides. This chip has several advantages over currently available techniques including speed, robust operation, and ability to process large volumes of sample and concentrate cells into a small end volume. Effusion specimens were prepared in only ten minutes, an order of magnitude faster than other similar techniques, with increased purity. The straightforward steps of device operation allowed for successful automation which reduces manual labor and minimizes user variation in sample preparation techniques.

Increased purity from chip processing also provides improved detection accuracy of mutations with qPCR. This system allows for rapid purification and isolation of cells of interest and has the potential to enable cytopathologists, clinicians, and researchers access to purified cells for preparing cytology slides, detecting specific gene mutations for targeted drug therapies, culturing cells for further analysis, or even isolating of single cells for next generation sequencing analysis at lower cost than currently available techniques. Improved mutational detection at lower cost from readily available body fluids provides a compelling route towards making targeted anti-cancer therapies a broad clinical reality.

References

[1] Sahn SA (1982) The differential diagnosis of pleural effusions. *West J Med*. 137(2): 99-108.

[2] Billah S, Stewart J, Staerkel G, Chen S, Gong Y, et al. (2011) EGFR and KRAS Mutations in Lung Carcinoma. *Cancer Cytopathol* 119: 111-117.

[3] Mach AJ, Adeyiga OB, Di Carlo D (2013) Microfluidic sample preparation for diagnostic cytopathology. *Lab Chip* 13: 1011-1026.

[4] Cross SE, Jin YS, Rao J, Gimzewski JK (2007) Nanomechanical analysis of cells from cancer patients. *Nat Nanotechnol* 2: 780-783.

[5] Gossett DR, Tse HTK, Lee SA, Ying Y, Lindgren AG, et al. (2012) Hydrodynamic stretching of single cells for large population mechanical phenotyping. *Proc Natl Acad Sci* 109: 7630-7635.

[6] Kassis J, Klominek J, Kohn EC (2005) Tumor microenvironment: What can effusions teach us? *Diagn Cytopathol* 33: 316-319.

[7] Hanahan D, Weinberg RA (2011) Hallmarks of cancer: the next generation. *Cell* 144: 646-674.

[8] Boldrini L, Gisfredi S, Ursino S, Tiziano C, Baldini E, et al. (2007) Mutational analysis in cytological specimens of advanced lung adenocarcinoma: a sensitive method for molecular diagnosis. *J Thorac Oncol* 2: 1086-1090.

[9] Malapelle U, de Rosa N, Rocco D, Bellevicine C, Crispino C, et al. (2012) EGFR and KRAS mutations detection on lung cancer liquid-based cytology: a pilot study. *J Clin Pathol* 65: 87-91.

[10] Molina-Vila MA, Bertran-Alamillo J, Reguart N, Taron M, Castellà E, et al. (2008) A sensitive method for detecting EGFR mutations in non-small cell lung cancer samples with few tumor cells. *J Thorac Oncol* 3: 1224-1235.

[11] Emmert-Buck M, Bonner RF, Smith PD, Chuaqui RF, Zhuang Z, et al. (1996) Laser capture microdissection. *Science* 274: 998-1001.

[12] Espina V, Wulfkuhle JD, Calvert VS, VanMeter A, Zhou W, et al. (2006) Laser capture microdissection. *Nat Protoc* 1: 586-603

[13] Chen J, Li J, Sun Y (2012) Microfluidic approaches for cancer cell detection, characterization, and separation. *Lab Chip* 12: 1753-1767.

[14] Saliba A-E, Saias L, Psychari E, Minc N, Simon D, et al. (2010) Microfluidic sorting and multimodal typing of cancer cells in self-assembled magnetic arrays. *Proc Natl Acad Sci* 107: 14524-14529.

[15] Gossett DR, Weaver WM, Mach AJ, Hur SC, Tse HTK, et al. (2010) Label-free cell separation and sorting in microfluidic systems. *Anal Bioanal Chem* 397: 3249-3267.

[16] Mach AJ, Kim JH, Arshi A, Hur SC, Di Carlo D (2011) Automated cellular sample preparation using a Centrifuge-on-a-Chip. *Lab Chip* 11: 2827-2834.

[17] Kimura N, Dota K, Araya Y, Ishidate T, Ishizaka M (2009) Scoring system for differential diagnosis of malignant mesothelioma and reactive mesothelial cells on cytology specimens. *Diagn Cytopathol* 37: 885-890.

[18] Kashii T, Mizushima Y, Monno S, Nakagawa K, Kobayashi M (1994) Gene analysis of K-, H-ras, P53, and retinoblastoma susceptibility genes in human lung cancer cell lines by the polymerase chain reaction/single-strand conformation polymorphism method. *J Cancer Res Clin Oncol* 120: 143-148.

[19] Morlan J, Baker J, Sinicropi D (2009) Mutation detection by real-time PCR: a simple, robust and highly selective method. *PloS ONE* 4: e4584.

Chapter 3: Rapid Enrichment of Circulating Tumor Cells for Enumeration

While the previous chapter focused on disseminated tumor cells (DTCs) found in pleural effusions, cells from stage IV cancer patients may occasionally be found at high enough concentrations and purities to facilitate ease of diagnostics in cytopathology without the need for significant enrichment. However, CTCs in blood are more extremely rare and must be enriched at higher efficiency with a minimum 4 orders of magnitude greater purity than the initial sample.

As mentioned in Chapter 1, many current technologies employ affinity-based capture methods, using antibodies or aptamers that bind to cell surface markers, but may potentially miss many CTCs that have undergone EMT and a downregulation of targetable cell surface markers. Inertial label-free size-based microfluidic devices have shown promise in isolating CTCs at higher throughputs, but are often not scalable and still suffer from low purities as well as dilute output sample volumes. Here, the Centrifuge Chip design was reconfigured and applied to blood samples in order to enumerate rare CTCs to aid patient prognostics.

Device modifications for high throughput blood processing

A series of design changes from the Centrifuge Chip were made to accommodate for blood processing. First, the efficiency of the design was doubled by fine-tuning the positioning of cells in microchannels. By increasing the cross-sectional aspect ratio (from 40×55 μm to 40×70 μm), inertial focusing of particles in straight channels reduces from 4 equilibrium positions to 2, toward the two larger faces of the channel, which brings particles closer to the vortex chamber and increases the likelihood of crossing the separatrix and becoming trapped [1]. Additionally, 10,000 μm long straight channels were added to the design to further increase particle focusing and trapping, resulting in the Vortex Chip design (Fig. 3.1).

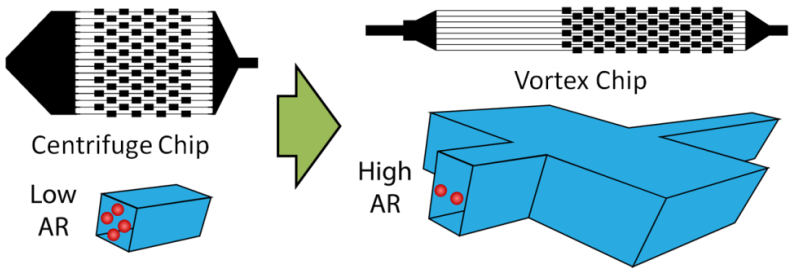

Figure 3.1: Design adjustments from Centrifuge Chip to Vortex Chip. In order to increase particle efficiency, channel height was increased from 55 μm to 70 μm to favor particle focusing to the 2 lateral side positions which are closer to vortex reservoirs. Additionally, long straight upstream channels were placed before reservoirs to ensure a sufficient distance for particles to become focused.

Subsequently, it was later demonstrated that the long upstream focusing channel of the Vortex Chip was found to be unnecessary for trapping. COMSOL software simulations demonstrates that the fluidic flow profile fully develops within a relatively shorter 500 μm minimum distance (Fig 1.7), suggesting that sufficient shear gradient lift forces are achievable over shorter distances. A 1000 μm straight channel distance between reservoirs was chosen to achieve a balance of high efficiency and purity (Fig. 3.2A). Accordingly, replacement of the long straight upstream focusing channel in the Vortex Chip with serial 1000 μm spaced reservoirs was found to improve cell capture (Fig. 3.2B). Next, parallelization from 8 to 16 channels enabled a 2x faster flow rate while maintaining the same Reynolds number (Fig. 3.2B). The final High-Throughput Vortex Chip design (Vortex HT)—used in experiments to generate the subsequent results—consisted of 16 parallel channels, each with an array of 12 reservoirs, totaling 3X more reservoirs and 2X higher operational flow rate (8 mL/min) than the previously described Vortex Chip (40).

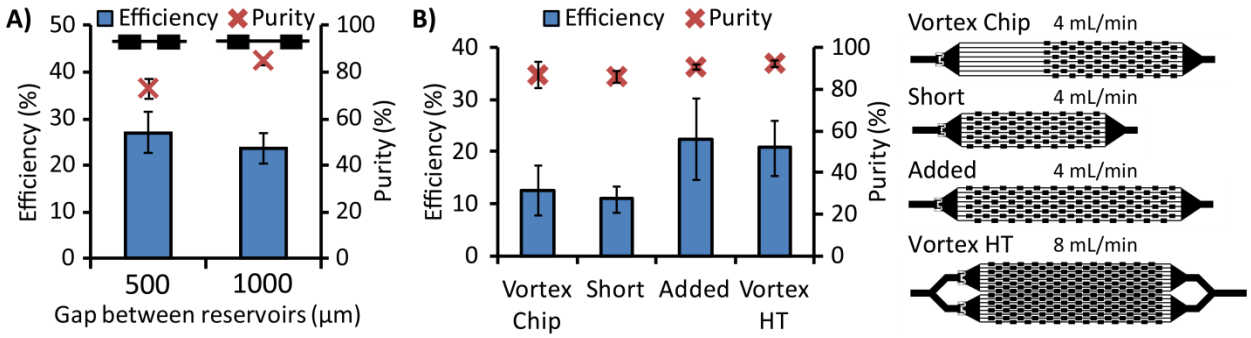

Figure 3.2: Optimization of device design for CTCs. **(A)** Reservoirs spaced 500 μm apart demonstrated higher capture efficiency of MCF7 cells spiked in 10x diluted blood, but at lower purity. The 1000 μm-spaced design was thus favored in subsequent designs. **(B)** The Vortex Chip consists of long upstream channels (10 mm) followed by 8 parallel channels, each with 8 capturing reservoirs. The Short design removes focusing channels while demonstrating comparable efficiencies (n = 3), and the Added design replaces each upstream channel with 4 more reservoirs for increased efficiency. Vortex HT is a parallelized version of the Added design and may operate at twice the flow rate (8 mL/min).

With the reduced time to process a sample using Vortex HT, saved time may be used to reprocess the fluid waste from the first trapping cycle to achieve higher capture efficiency for cancer cells. In the same processing time as the Vortex Chip, Vortex HT recovers cells at 1.6x higher efficiency using 2 cycles of processing (Fig. 3.3A) while maintaining high sample purity (>80%). Recovery is further enhanced by multiple rounds of reprocessing (with a trade-off of increased run time), resulting in up to 84% cumulative efficiency after 7 processing cycles of 4 mL of 10x diluted blood spiked with 600 MCF7 cells (Fig. 3.3B). Interestingly, efficiencies remain comparable per cycle, suggesting that the entry and maintenance of cells in vortex traps is a probabilistic process. The captured cells remain viable and may be collected directly off-chip in a concentrated ~150 μL volume per run. Cells were spun down, incubated with media, and viability tests were performed each day on a different well of the cell population using Calcein Blue AM and ethidium homodimer (Molecular Probes). MCF7 cells were able to be cultured for over 4 days (Figs. 3.3C, 3.3D) at which point the experiment was stopped.

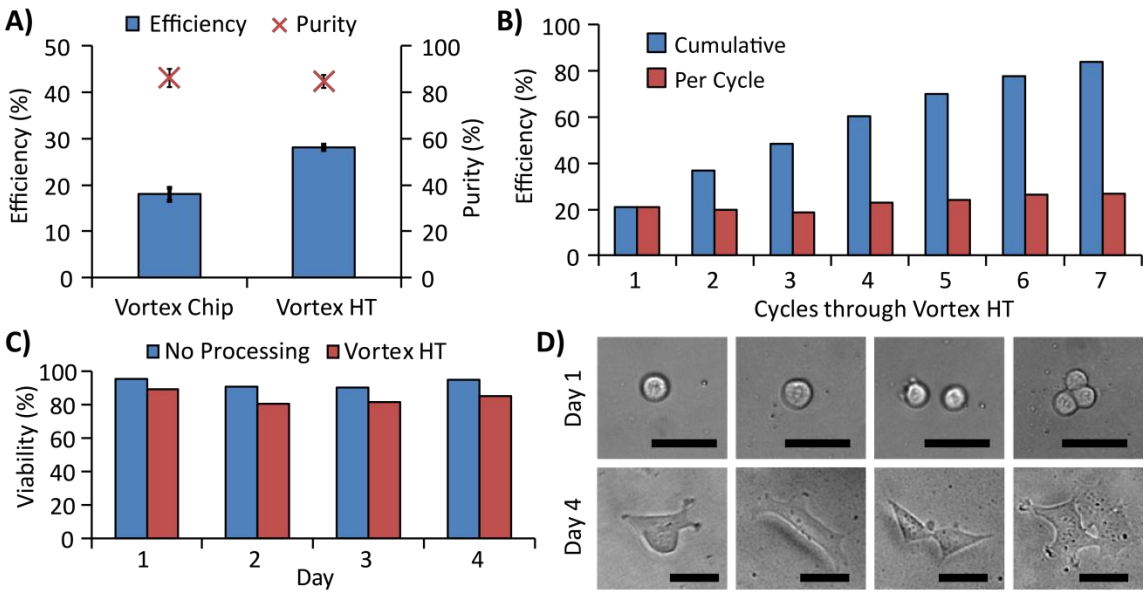

Figure 3.3: Device performance with cell lines. (A) Comparison of device efficiencies for the same processing time. Vortex HT yields ~1.6x higher capture efficiency of MCF7 breast cancer cells while maintaining comparable purity (n=3 trials). **(B)** Sample flow-through may be collected and repeatedly processed through multiple cycles to increase cell capture with a tradeoff of slightly diminished sample purity. **(C)** MCF7 cells processed through Vortex HT maintained high relative viability compared with cells not processed through the device. **(D)** MCF7 cells released into a well-plate are able to grow and proliferate for over 4 days. Scale bar represents 40 μm.

Immunofluorescent staining and classification criteria

Once purified cells are collected, an additional emerging challenge lies with cellular characterization after enrichment. Although size-based isolation approaches may acquire subpopulations of cells that have undergone EMT or other trans-differentiation processes, collected cells can be difficult to identify with commonly used stains optimized for cells of epithelial origin (e.g. cytokeratins). Studies have found irregular CTC expression profiles in which epithelial (CK, EpCAM), mesenchymal (vimentin, N-cadherin), or potentially either both or neither markers are expressed [2-4]. Additionally, non-specific binding of probes may result in cross-reactivity and cause difficulties in proper cell identification. The CellSearch CellTracks Analyzer II semi-automated system aids in CTC identification, but it is dependent on CK expression, and high variability occurs between trained operators [5,6]. Finally, variability of

staining protocols, antibody clones between vendors, and imaging setups causes conflicting definitions of CTCs. A more general, standardized staining and classification approach is required, which takes into account cells that are negatively- or doubly-stained for standard epithelial markers. Cytomorphological characteristics, such as abnormal cell size and large nuclear-to-cytoplasmic (N:C) ratios, are also indicators of malignancy or hematopoietic origins that may be factored in with high quality imaging for cell identification. Due to differences in implementing immunofluorescence staining and counting protocols between labs, a standardized classification approach should be rigorously described and demonstrated with galleries of images and detailed training documents.

Based on standard CK and CD45 immunostaining and morphological features that are diagnostic in cytopathology, a set of criteria was developed to classify cells (Fig. 3.4). Classifications were comprised of 3 categories: debris, WBCs, or CTCs. In general, debris was characterized by irregular, jagged shapes or dark outlines under bright-field microscopy. Aside from the clear distinctions of CTCs as CK+/CD45-/DAPI+ and WBCs as CK-/CD45+/DAPI+, incidences arise in which cells may be doubly-stained (CK+/CD45+/DAPI+) or DAPI+ only. Staining with CD66b-AlexaFluor647 (CD66b-AF647, Clone G10F5, BD Biosciences) confirmed that doubly-stained cells corresponded to activated granulocytes, and were thus classified as WBCs. For instances in which cells stained DAPI+ only, WBCs were distinguished by lobular or segmented granulocytic nuclei, small nuclei (<9 μm), and/or small N:C ratios. CTCs were primarily characterized by a large nucleus (>9 μm) and large N:C ratio.

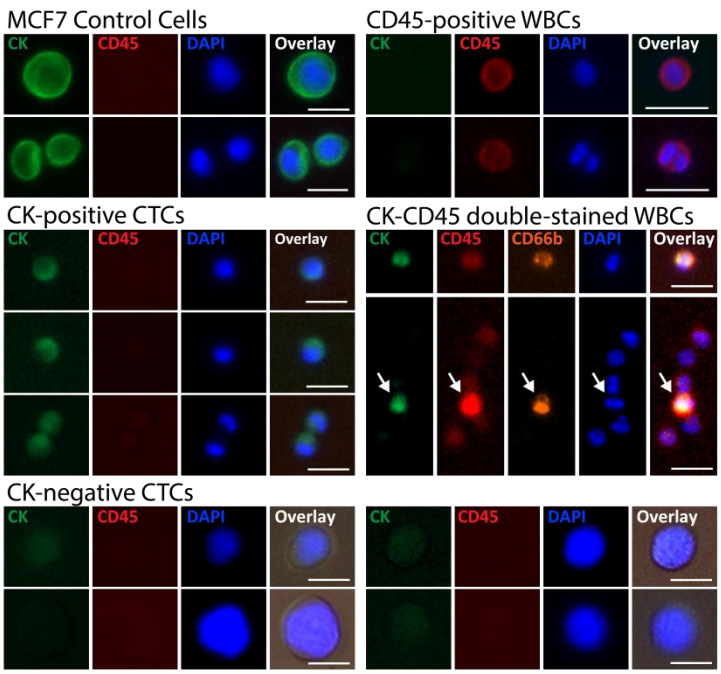

Order	Characteristic	Type	Ex.
1	Atypical shape or dark fill/outline	Debris	
2	CD45+/DAPI+/CK-	WBC	
3	CK+/DAPI+/CD45-	CTC	
4	Lobed Nucleus	WBC	
5	CK+/CD45+/DAPI+	Favor WBC	
6	Nucleus < 9 μm	WBC	
7	Nucleus > 9 μm, N:C ratio < 0.60	WBC	
8	Nucleus > 9 μm, N:C ratio > 0.60	CTC	

Figure 3.4: **Immunofluorescent staining and classification criteria.** Collected cells were classified according to immunostains against CK (green) and CD45 (red), as well as DNA stained with DAPI (blue). CTCs were defined as either CK+/CD45-/DAPI+ or DAPI+ only with a large nucleus (>9 μm) and N:C ratio (>0.60). Each cell was compared with the table's criteria in the order listed until the characteristics matched. Scale bars represent 20 μm and 10 μm in the gallery and table, respectively.

Enumeration of patient samples with Vortex technology

The staining and classification criteria technique was used to enumerate CTCs from patient samples. Blood was acquired in two 10 mL EDTA-coated tubes (Vacutainer, BD) from consenting stage IV lung and breast cancer patients collected from the UCLA Hematology and Oncology Santa Monica Clinic and Stanford Medical Center as well as from age-matched healthy donors following institutional review board approved protocols (UCLA IRB#11-001798 and Stanford IRB#5630). Within 4 hours of procurement, one tube of whole blood was diluted 10x in PBS before processing through Vortex HT with 2 cycles, and enriched cells were collected in a 96-well plate, immunostained, imaged, and manually enumerated. The second tube of blood from the same patient was processed through either the previous Vortex Chip [7] or the gold standard CellSearch assay (performed by Quest Diagnostics). All samples were de-

identified by a clinical coordinator and research staff was blinded to the sample type (between lung, breast, or healthy blood samples). CTC counts from cancer samples were compared with the maximum enumerated value from healthy samples to determine which patients have tested positive for CTCs using Vortex HT.

A total of 22 breast, 15 lung, and 10 age-matched healthy blood samples were used in the study. The majority of cancer patients (36/37) were undergoing treatment at the time of draw. Using the classification criteria, more CTCs were found in lung (mean: 5.3 CTCs/mL, range: 0.5-24.2 CTCs/mL) and breast (mean: 5.4 CTCs/mL, range: 0.75-23.25 CTCs/mL) cancer samples than in healthy controls (mean: 0.56 CTCs/mL, range: 0-1.25 CTCs/mL) (Fig. 3.5A). A low number of cells were characterized as CTCs in healthy samples, with a maximum count of ~1.25 CTCs/mL. Using this baseline value as a threshold, approximately 80% and 86% of lung and breast cancer samples, respectively, were found to be positive for CTCs. The captured CTCs displayed varying levels of CK expression, with 40.8% of total CTCs not expressing CK at all (Fig. 3.5B). Interestingly, this percentage was not reflected at the individual patient level. There was significant heterogeneity between patients with a bimodal distribution of patients with either high levels of CK+ CTCs or low levels of CK+ CTCs (Fig. 3.5C).

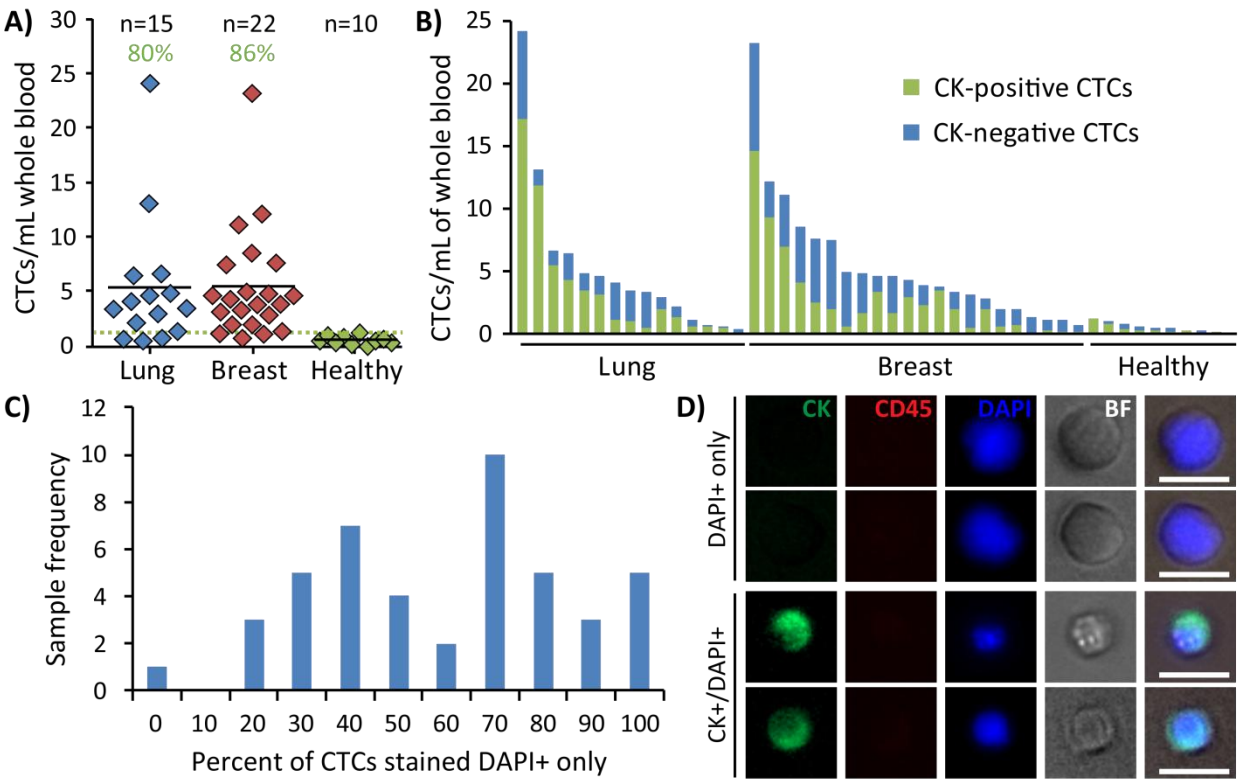

Figure 3.5: Immunostaining characteristics of patient CTCs. **(A)** More CTCs/mL of whole blood were found in stage IV metastatic lung (n=15) and breast (n=22) cancer blood samples than in age-matched healthy samples (n=10). Based on the maximum count for all healthy samples, a minimum threshold of 1.25 CTCs/mL of whole blood (dotted green line) was set to define samples as CTC-positive. Using such a threshold, approximately 80% and 86% of lung and breast cancer samples, respectively, were found positive for CTCs. **(B)** CTCs collected from each patient sample were composed of both CK-positive (green) and CK-negative (DAPI+ only, blue) subpopulations. **(C)** Stained samples exhibited a roughly bimodal distribution in which the majority of cells in each sample were either stained positive for DAPI only or positive for CK, but not in equal numbers. **(D)** Representative images of DAPI+ only cells and CK+/DAPI+ stained cells. Scale bar represents 20 μm.

One healthy donor self-reported diagnosis with chronic myelogenous leukemia (CML) 20 days after having blood drawn for the study, and this patient was removed from the analysis of healthy samples. Interestingly, very large cytomorphologically atypical WBCs were found after processing with Vortex HT, before the patient was treated (Fig. 3.6). The cells were characterized by a range of N:C ratios, but all were over 20 μm in diameter and CD45+/DAPI+/CK-/CD66b-. An additional sample of blood was later acquired from the same

patient during treatment. Complete blood counts (CBCs) of the patient showed a high concentration of WBCs (40.9 K/μL), far above the normal range expected in a healthy patient (4-11 K/μL), and later decreased to 3.1 K/μL while under treatment (Fig. 3.6C). In a similar trend, fewer atypical WBCs were captured from Vortex HT in the second draw. No such atypical white blood cells were seen in healthy donor samples, nor in lung or breast cancer patient samples, which may suggest the utility for Vortex HT as a general approach to enrich for other large circulating cells useful for the detection and analysis of other diseases.

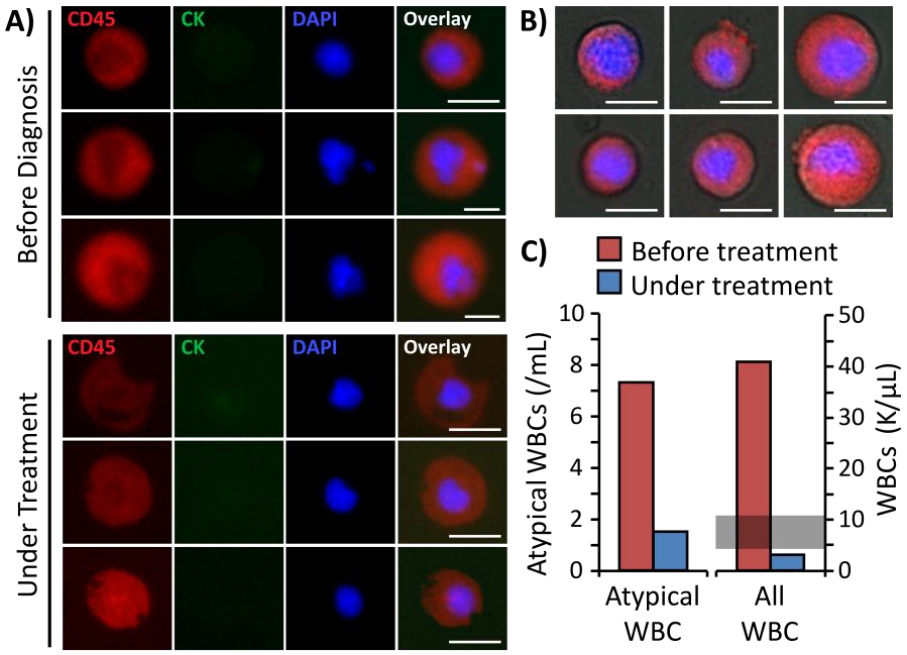

Figure 3.6: Case study of a leukemia patient. **(A)** Large atypical CD45+/DAPI+ WBCs were found in the blood from a leukemia patient. Very large atypical cells (30-40 μm) were found before the patient was diagnosed, and smaller but consistently large atypical cells (~20 μm) were found from the same patient while under treatment. **(B)** All atypical WBCs exhibited large nuclei (~15 μm) but varying nuclear-to-cytoplasmic ratios. All scale bars represent 20 μm. **(C)** The number of atypical white blood cells isolated from Vortex HT decreased on the second draw after the patient started treatment. Similarly, CBC data show that the total number of WBCs decreased. The normal expected range for WBC concentration is shaded in gray.

Comparisons of Vortex performance with other technologies

Vortex HT enriched for a larger number of CTCs than the Vortex Chip in all 7 lung and 7 breast cancer patient samples tested, using the same volume of sample and same processing time

for each device (Fig. 3.7A). Notably, the numbers of CTCs captured with Vortex HT correlated with the number of CTCs isolated with the Vortex Chip (R^2 =0.92, slope=1.44). That is, samples with larger CTC numbers captured by Vortex Chip had concomitantly larger capture numbers by Vortex HT. These results also demonstrated the chip-to-chip concordance of this processing approach, which suggests minimal variation induced by the capture technology itself.

For 13 cancer patient samples tested with CellSearch, Vortex HT found 85% positive for CTCs above a healthy patient cut-off whereas CellSearch found only two samples (15%) positive above the healthy patient cut-off value for that system (Figs. 3.7B, 3.7C). Moreover, the number of CTCs captured in these two samples (breast sample no. 5 and 6, Fig. 3.7B) were markedly different between CellSearch and Vortex HT, which is likely due to the differing selection parameters of EpCAM expression with CK positivity versus cell size and a combination of immunofluorescence and morphological features. Because of the reduced expression of EpCAM in lung tumor cells, CellSearch is not FDA approved for analysis of lung cancer patient samples, which explains the poor results. Two other samples (starred, Fig. 3.7B) exhibited issues with the CellSearch instrument, which displayed the error "Machine aborted sample during run", and were deemed as uninterpretable for CTCs by the test system.

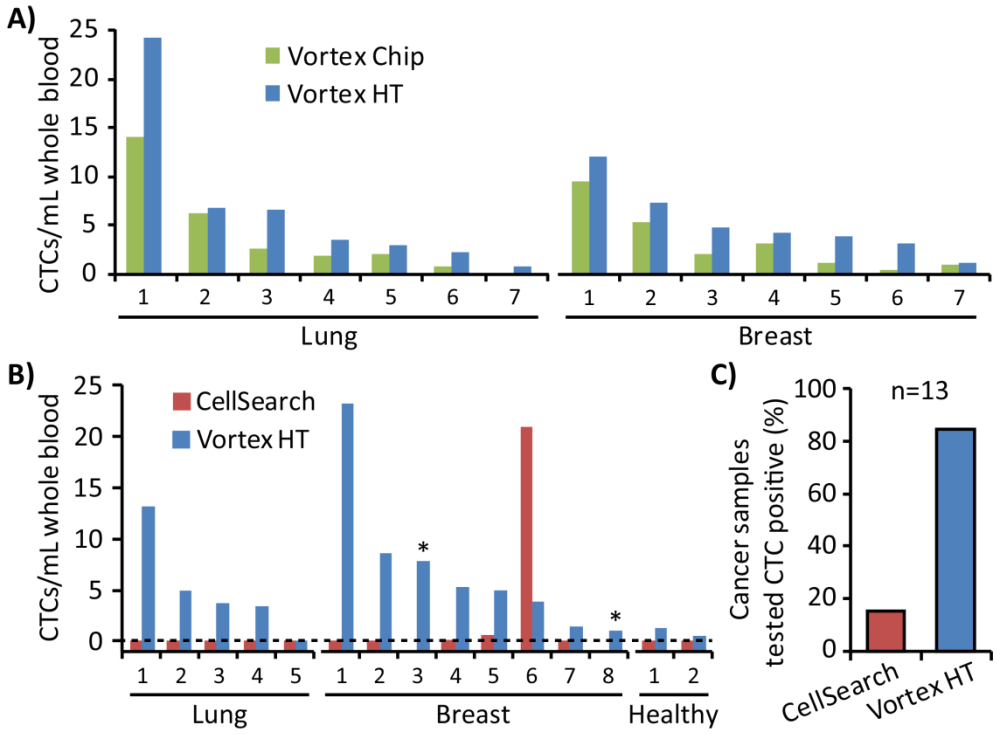

Figure 3.7: Comparison of Vortex HT with other technologies. (A) Vortex HT captures more CTCs than the Vortex Chip in all cases (7 lung and 7 breast). **(B)** Blood tubes from the same patient were split for tests between Vortex HT and CellSearch for 5 lung, 8 breast, and 2 healthy samples. In two breast patients (3 and 8, starred), the test was aborted by the CellSearch machine. **(C)** In 13 of the metastatic cancer patient samples tested, the CellSearch test identified CTCs in 15% of samples, whereas Vortex HT found 85% of samples as positive for CTCs above levels for age-matched healthy controls.

Concluding remarks

At an operational flow rate of 8 mL/min, Vortex HT maximizes throughput while maintaining high purity and cell viability. The simple geometry of the device, consisting only of straight microchannels and rectangular trapping regions, enables straightforward device fabrication and sample processing procedures. With minimal pretreatment steps that may damage cells, one vial of blood (~8 mL) may be processed in 2 cycles within a short ~20 min period, yielding demonstrably higher CTC counts in cancer patient specimens over healthy blood and a higher positive success rate compared with CellSearch. Since cells remain viable and are released at a low, concentrated volume (~150 μL), Vortex HT may enable diverse downstream

analyses of rare CTCs, including single-cell sequencing or RT-PCR, cytogenetic analyses, cell culture and pharmacological studies [8], and single-cell Western blotting [9]. Moreover, the device provides a convenient sample preparation step that may be streamlined with cytopathology or immunocytochemistry techniques, in which technicians are often burdened by low sample purity. The purity achieved with Vortex HT may also facilitate CTC genotyping in a step toward new drug discovery, personalized medicine, and informed treatment decisions for patients. In addition to lung and breast cancer CTCs, the size-based isolation platform may potentially be applied for a variety of other cancer types (prostate, colon, melanoma, bladder cancer, etc.), or even other cell types (tumor cells, stem cells, endothelial cells, etc.) within a variety of biofluids (blood, urine, pleural and peritoneal fluid, etc.).

The presence of atypical WBCs from a CML patient sample suggests that Vortex HT may also isolate large leukemic blasts. As CML cells range in size, with ~35% of cells in the range of 14-35 μm [10], Vortex HT may be effective in purifying rare subpopulations of large cells which may otherwise remain hidden from affinity-based capture approaches. Although it remains unclear if the isolated cells are malignant cell precursors, immature white blood cells, or apoptotic cells, the absence of such cells from lung, breast, and healthy donor samples suggest their unique role in CML. These preliminary findings suggest further work is warranted to evaluate Vortex HT as an enrichment tool for a more sensitive identification of patient state that may be important for minimal residual disease monitoring. While relatively little microfluidic work has focused on sample preparation for observing and diagnosing CML [11], current techniques of isolation by dielectrophoresis [12], aptamer-based probes [11], or viscoelastic properties of cells [13] remain time-consuming or not fully developed; Vortex HT may offer a high throughput, label-free means for leukemia cell purification. More broadly in a screening

role, Vortex trapping from blood that yields an atypical large cell count may provide an earlier indication of a brewing disease process for a range of disease states [14], suggesting additional diagnostics to define the source of the large circulating cells may be warranted for the patient.

The objective cell identification criteria presented here addresses common but widely unreported concerns surrounding immunostains. Since many cells may transition to a mesenchymal state [14], traditional epithelial cell staining techniques may overlook a significant number of candidate cells [15], resulting in underreported performances especially in size-based isolation platforms. While most devices are characterized using probes for CK, CD45, and DAPI, we expect the introduced CTC identification criteria that also take advantage of the accumulated knowledge of structural features associated with malignancy by cytopathologists will complement future device performance characterizations, clinical applications, and help standardize existing commercial prognostic and sample preparation tools as well as those in development. To help others who wish to adopt these tools, we provide a comprehensive guide and training worksheets (Supplementary Material) to more effectively convey our accumulated knowledge. As with most available techniques, the introduced enumeration protocol is not fully comprehensive and does not factor in the use of other marker types, including those that are cancer origin-specific (e.g., anti-HER2 staining for breast cancer samples, or anti-PSA for prostate cancer). We expect that the presented criteria will help foster future discussions regarding proper validation of CTCs, and envision that the described criteria can serve as a starting point for further adaptations to the method as promising new markers or automated imaging software become available.

References

[1] S. C. Hur, H. T.K. Tse, and D. Di Carlo, Sheathless Inertial Cell Ordering for Extreme Throughput Flow Cytometry, *Lab Chip*, 2010, **10,** 274-280.

[2] Yu M, Bardia A, Wittner BS, Stott SL, Smas ME, Ting DT, et al. Circulating Breast Tumor Cells Exhibit Dynamic Changes in Epithelial and Mesenchymal Composition. *Science*. 2013;339:580–4.

[3] Armstrong AJ, Marengo MS, Oltean S, Kemeny G, Bitting RL, Turnbull JD, et al. Circulating tumor cells from patients with advanced prostate and breast cancer display both epithelial and mesenchymal markers. *Mol Cancer Res*. 2011;9:997–1007.

[4] Satelli a., Brownlee Z, Mitra a., Meng QH, Li S. Circulating Tumor Cell Enumeration with a Combination of Epithelial Cell Adhesion Molecule- and Cell-Surface Vimentin-Based Methods for Monitoring Breast Cancer Therapeutic Response. *Clin Chem*. 2014;61:259–66.

[5] Riethdorf S, Fritsche H, Müller V, Rau T, Schindlbeck C, Rack B, et al. Detection of circulating tumor cells in peripheral blood of patients with metastatic breast cancer: a validation study of the CellSearch system. *Clin Cancer Res*. 2007;13:920–8.

[6] Miller MC, Doyle G V, Terstappen LWMM. Significance of Circulating Tumor Cells Detected by the CellSearch System in Patients with Metastatic Breast Colorectal and Prostate Cancer. *J Oncol*. 2010;2010:617421.

[7] Sollier E, Go DE, Che J, Gossett DR, O'Byrne S, Weaver WM, et al. Size-selective collection of circulating tumor cells using Vortex technology. *Lab Chip*. 2014;14:63–77.

[8] Yu M, Bardia A, Aceto N, Bersani F, Madden MW, Donaldson MC, et al. Ex vivo culture of circulating breast tumor cells for individualized testing of drug susceptibility. *Science*. 2014;345:216–20.

[9] Hughes AJ, Spelke DP, Xu Z, Kang C-C, Schaffer D V, Herr AE. Single-cell western blotting. *Nat Methods*. 2014;11:749–55.

[10] Lozzio CB, Lozzio BB. Human chronic myelogenous leukemia cell-line with positive Philadelphia chromosome. *Blood*. 1975;45:321–34.

[11] Pratt ED, Huang C, Hawkins BG, Gleghorn JP, Kirby BJ. Rare cell capture in microfluidic devices. *Chem Eng Sci*. 2011;66:1508–22.

[12] Imasato H, Yamakawa T, Eguchi M. Separation of Leukemia Cells from Blood by Employing Dielectrophoresis. *Intell Autom Soft Comput*. 2012;18:139–52.

[13] Wang G, Crawford K, Turbyfield C, Lam W, Alexeev A, Sulchek T. Microfluidic cellular enrichment and separation through differences in viscoelastic deformation. *Lab Chip*. 2015;15:532–40.

[14] Bethel K, Luttgen MS, Damani S, Kolatkar A, Lamy R, Sabouri-Ghomi M, et al. Fluid phase biopsy for detection and characterization of circulating endothelial cells in myocardial infarction. *Phys Biol*. 2014;11:016002.

[15] Chinen LTD, de Carvalho FM, Rocha BMM, Aguiar CM, Abdallah EA, Campanha D, et al. Cytokeratin-based CTC counting unrelated to clinical follow up. *J Thorac Dis*. 2013;5:593–9.

Chapter 4: Mechanophenotyping of Rare Cells for Label-Free Enumeration

As noted in the previous chapter, the CTC field has revolved around two steps, which require the need to i) enrich for CTCs, and ii) identify the CTCs in the enriched sample. While current label-free technologies have only focused on CTC enrichment, the use of affinity-based immunofluorescence (IF) has remained the universal gold standard for the second step of identifying captured CTCs, in which fluorescent probes specifically bind to cell surface markers commonly found on cells of epithelial origin. However, the IF process itself has inherent complications due to the wide heterogeneity of cellular biomarker expression and the lengthy > 3 hrs of staining, imaging, and manual enumeration. Ideally, a completely label-free technique would be a powerful and affordable alternative to assay all types of cells, including EpCAM positive, EpCAM negative, EMT-associated, and platelet-coated cells. This chapter explores label-free biophysical characterization of tumor cells and establishes the first reported deformability measurements and label-free enumeration of rare CTCs.

Cell biophysics as a means for characterizing cells

Aside from the use of antibodies to target heterogeneous surface antigens, the intricacies of gene expression and cellular behavior may alternatively be encompassed by measurable biophysical parameters, such as cell deformability [1]. Quantification of CTC deformability may yield powerful correlations with patient information, such as staging, cancer type, or likely sites for secondary metastases. Of immediate interest, the biophysical profile of CTCs may uniquely distinguish them from other cell types present in blood, which allows for automated cell enumeration, an essential component in determining cancer patient prognosis and disease progression.

Several devices have been developed to sort and characterize cells based on deformability, such as measuring the time of cancer cell passage through narrow channel constrictions [2,3], driving cells through pinched flow streams to measure hydrodynamic stretching [4,5], using optofluidic laser technology for single-cell stretching and sorting [6], or driving cancer cells through resettable cell traps [7]. While these technologies have been demonstrated on abundant cultured cancer and stem cells, the biophysics of native primary CTCs have yet to be specifically quantified, which may be due to the fact that CTCs are extremely rare; any sample collected and transferred between enrichment and characterization devices may yield significant cell losses due to cell adhesion (e.g. in microchannels, tubing, fluid carriers, pipette tips, etc.). Additionally, the purity of enriched CTC samples may also impede single cell biophysical measurements and limit device throughput.

One existing technology, known as deformability cytometry (DC) [8,9], makes use of two fluid streams which collide in an inertial microfluidic extensional flow junction, at which cells are stretched at high throughput (>2,000 cells/s). Cellular deformations are visualized and resolved with a high speed camera, and an automated script measures their deformability, defined as the aspect ratio of the distances between the long axis to minor axis of the elliptical cell at maximum deformation. The technology has been applied to study stem cells [8] and identify malignant pleural effusions, which tend to have high cellularity [9]. Ideally, the integration of an upstream Vortex CTC isolation platform with a downstream mechanophenotyping DC platform with minimal cell loss may address some key challenges. However, device integration is non-intuitive and leads to several challenges, primarily due to the difficulty of handling rare single cells; in particular: i) maintaining the correct operational flow rate to achieve all steps necessary (device priming, sample infusion, wash, cell release, cell deformation, etc.) without losing cells during the process or generating excess pressures that could delaminate or burst devices, ii) minimizing cell loss from incorrect timing in

video recordings which may miss single cell events, or low efficiency of obtaining usable measurements from each single CTC, and iii) achieving high throughput and rapid deformability measurements of cells, which ideally requires all cells to be resolved in one video.

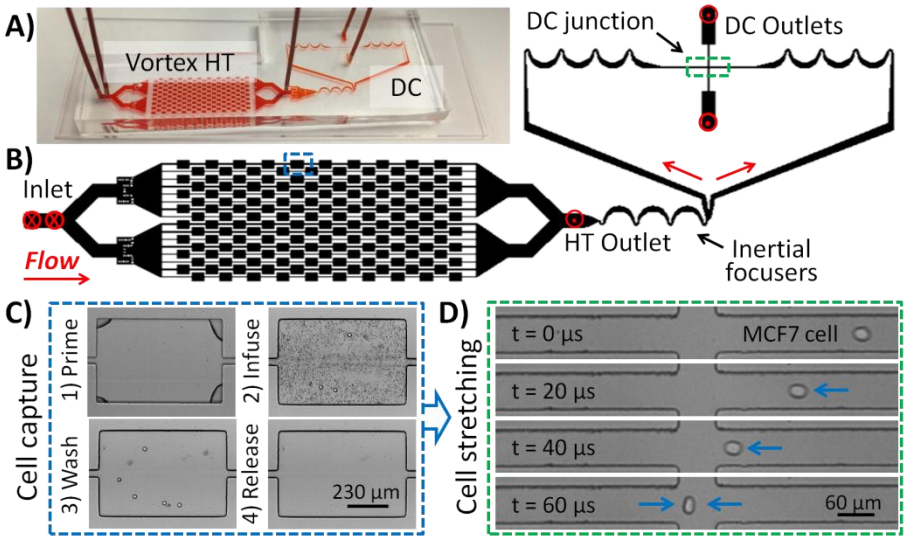

Figure 4.1: Vortex-mediated deformability cytometry. (A) VDC is a simple glass-bonded PDMS device. **(B)** It contains 2 inlets for sample and wash buffer, and 3 outlets. Fluid waste passes through the HT outlet during cell capture, and cells pass through the DC junction and out the 2 DC outlets during cell release. **(C)** Cell capture requires the same process as Vortex HT. **(D)** Upon release, cells pass through the DC junction, where high speed imaging records cell deformation.

Cellular biophysical characterization with Vortex-mediated deformability cytometry

An integrated PDMS device and workflow was developed to combine Vortex HT with DC. The resulting vortex-mediated deformability cytometry (VDC) device (Fig. 4.1A) consists of two components: i) a 70 µm-deep Vortex HT region consisting of 16 parallel channels and 160 total rectangular trapping reservoirs, and ii) a 35 µm-deep DC region with inertial focusing channels which orient cells to be stretched at an extensional flow junction [8,9]. Similar to the previous chapter's Vortex HT device, the VDC device has two inlets for PBS wash buffer and sample. Between the two regions lies an HT outlet through which fluid waste flows during priming, sample infusing, and solution exchange (Fig. 4.1B). Once cells are captured in the reservoirs and excess blood cells (WBCs) are washed away (Fig. 4.1C), the HT outlet is briefly

closed (~1 s), causing a sudden pressure increase that disrupts vortices and releases cells toward the DC portion of the device. The DC region of the device contains asymmetric curving channels which make use of Dean vortices to first focus cells toward one side of the device, and then focus cells to a single stream in which they may be oriented toward the center of the channel prior to the DC junction. Cells at the junction are imaged at 100x magnification with a high speed camera (Vision Research Phantom v711) at ~500,000 fps, and pass to the outlets to be collected (Fig. 4.1D). Each video recording adds up to ~1.5 GB of 208×32 pixel resolution data in a 1.2 s time interval, which is sufficient to resolve cellular deformations.

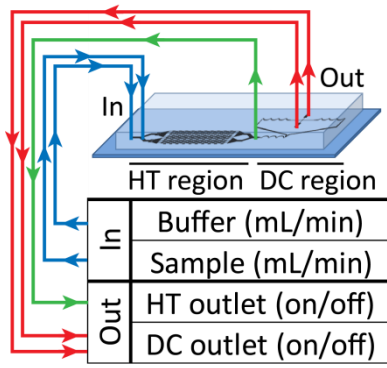

		Prime	Pressurize	Infuse	Wash	Stabilize	Release	Flush
		60s	30s	150s	15s	5s	1s	60s
In	Buffer (mL/min)	1	8	1	8	8	8	1
In	Sample (mL/min)	0	0	7	0	-0.5	0	0
Out	HT outlet (on/off)	✗	✓	✓	✓	✓	✗	✗
Out	DC outlet (on/off)	✓	✗	✗	✗	✓	✓	✓

Figure 4.2: VDC process flow. Samples are processed in a series of logical steps, which require: i) priming the device to fill channels with fluid, ii) pressurizing the chambers at high flow rate to prevent contaminating back-flows, iii) infusing patient sample to capture CTCs in vortices, iv) washing the reservoirs to remove unstably trapped smaller cells, v) stabilizing the sample syringe to avoid residual blood leakage, vi) releasing the cells from vortices and into the DC region of the device, and vii) flushing the system to ensure all cells are released into the downstream collection vessel. Solution flow rates and outlet valving must be controlled for each step.

The specific VDC process flow is outlined in Figure 4.2. While the typical prime, infuse, wash, and release steps mirror the procedure for Vortex processing, a few additional considerations must be made for the different outlets. The priming step takes place one time before the experiment begins, and requires a low flow rate to pass through the device to ensure all air bubbles are removed. Next, pressurization occurs at high flow rate with the DC outlets closed. Over the course of 30 s, the PDMS chambers become pressurized, and flow fully

develops and exits the HT outlet. This step ensures that no residual blood cells will enter the DC region of the device. The sample is then infused through the device at an overall 8 mL/min, and fluid waste passes through the HT outlet. The wash step occurs with a solution exchange at the same flow rate, and stabilization is needed to release some pressure from the sample syringe to prevent residual flow of blood cells through the chambers during the wash. During this time, the DC outlets are opened and guided to the well plate. Cell release occurs when the HT outlet is closed at the same time as the video recording is triggered. Cells are released from the vortices in a quick ~0.5s time interval (Fig. 4.3A) and immediately pass through to the DC junction, also within a quick ~0.5s time interval (Fig. 4.3B). Cells released in this manner maintain an average speed of 4.74 ± 0.93 m/s which is sufficient to observe deformations (Fig. 4.3C). With the DC outlets still open and placed over the well, the device is flushed with PBS to ensure release of cells into the well plate. The integrated device exhibits minimal cell loss, with 98.7% ± 1.5% (n = 4) of cells passing from the Vortex HT region to the DC region. Moreover, the number of cells observed in the DC junction matches closely with the number of cells observed in the well plate, and each run yielded close to 40% capture efficiency of MCF7 cells spiked in 10x diluted blood (Fig. 4.3D). Additionally, collected cells remain viable and may be grown in culture for > 6 days (Fig. 4.3E).

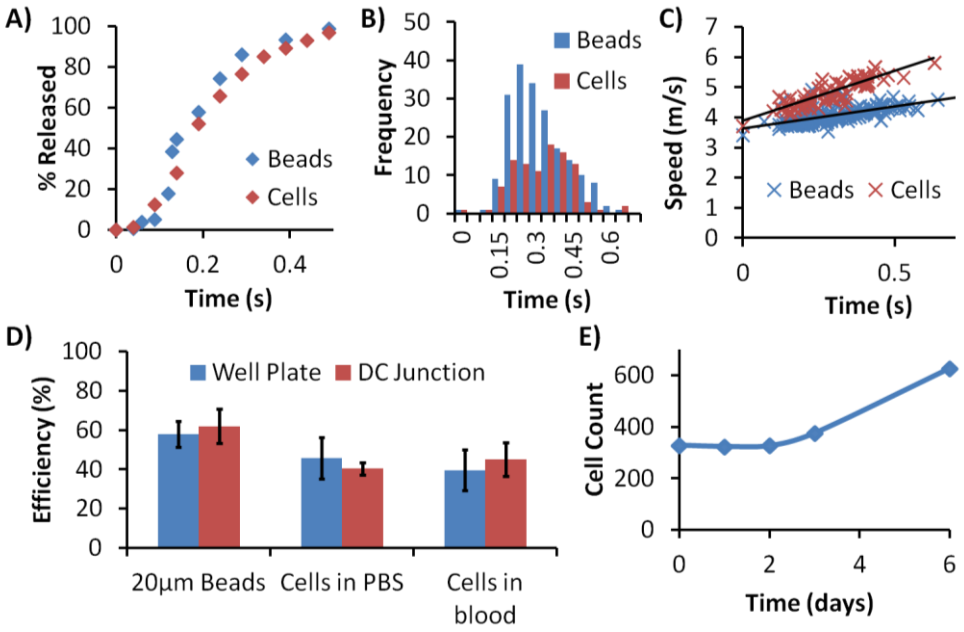

Figure 4.3: VDC device performance. Beads and cells are released from vortices in a quick <0.5 s time interval **(A)**, and also pass through the DC junction in <0.5 s **(B)**, which allows all cells to be imaged in one high speed video. **(C)** The speed of cells slightly increases over the course of their release, but is a high enough velocity to observe and resolve deformations. **(D)** The number of particles observed in VDC videos matches closely with the number captured in the well plate, and samples spiked with MCF7 cells reveal ~40% capture efficiency. **(E)** Cells collected in the well plate are still viable and may be cultured and grown for over 6 days.

Identification of CTCs from patient samples

Scatterplots of deformability vs. size of cells (Figs. 4.4A-C) reveal different populations between healthy blood (n = 5) and stage IV lung and breast cancer blood samples (n = 16). In both cases, a population of small 10 µm WBCs with average ~1.2 deformability is seen. Moreover, a scattered group of larger (>15 µm), more rigid (<1.2) cells is observed in both sample types, which may represent large WBCs (e.g. macrophages) or other large circulating cells. Finally, a unique population of large (>15 µm) and deformable (>1.2) cells is observed only from cancer blood samples (Fig. 4.4B), suggesting that they are CTCs or cancer-associated cells. By setting user-guided cutoffs for both size and deformability, the dataset was calibrated by support vector machine (SVM) processing to define a threshold above which defines a CTC.

Based on the threshold, cells were categorized into CTC and WBC groupings. CTCs tended to be larger and more deformable (Figs. 4.4D-F) than WBCs. CTCs had similar deformability and size ranges as MCF7 breast cancer cells (Fig. 4.4G).

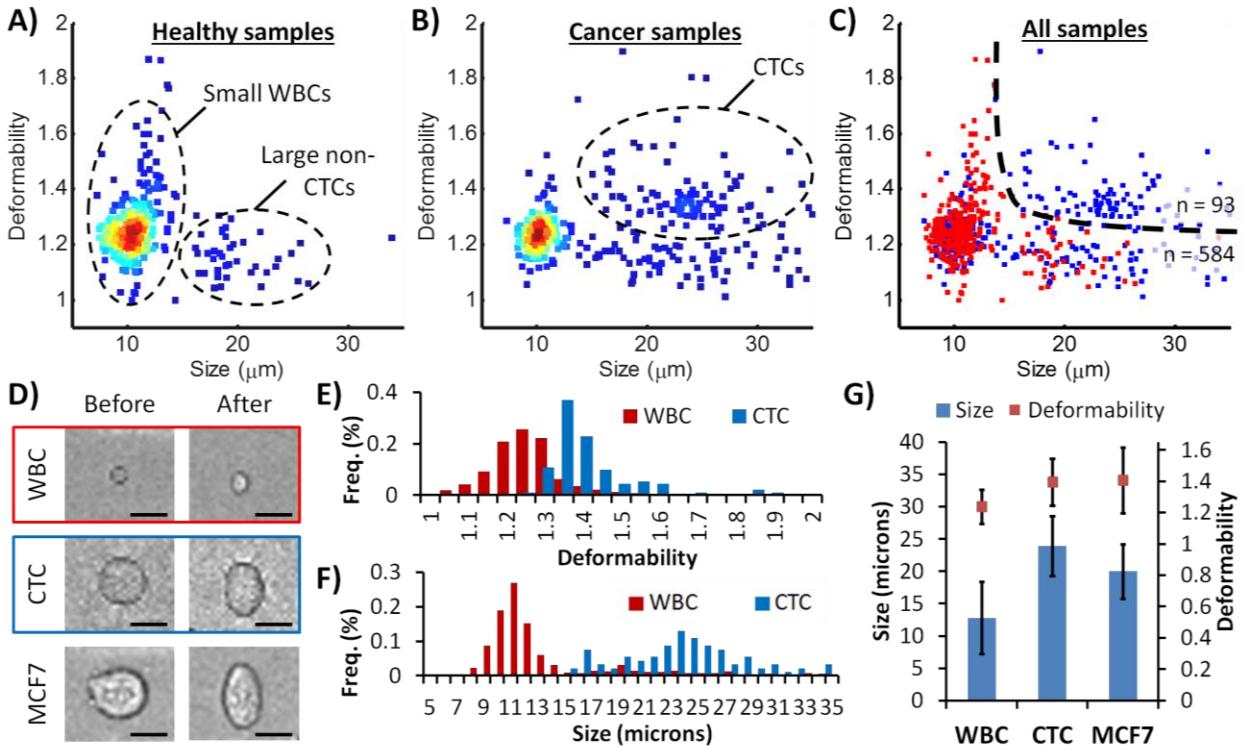

Figure 4.4: Enriched cell profiles from patient samples. (A) 5 healthy samples were processed with VDC and revealed populations of small WBCs and large non-CTCs with low deformability. **(B)** Samples from 16 cancer patients revealed a population of large, deformable CTCs. **(C)** Setting a threshold with SVM on cancer patient cells (blue) and healthy donor cells (red), 93 cells from all patients were identified as CTCs. **(D)** Examples of typical cells observed in high speed VDC videos before and after deformation. CTC populations were generally more deformable **(E)** and larger **(F)** than WBC populations. **(G)** CTCs also exhibited similar biophysical profiles as the MCF7 breast cancer cell line.

Cells assayed through VDC were also collected off-chip and immunostained with CK-FITC, CD45-PE, and DAPI to verify the presence of CTCs and correlate to DC measurements. Similar to the Vortex HT device from the previous chapter, populations of CK+/DAPI+ and large CK-/DAPI+ CTCs were present from samples processed by VDC (Fig. 4.5A), with about 47% of CTCs staining negative for CK. The number of CTCs defined by VDC thresholding

correlates strongly with the number of CTCs identified by IF (Fig. 4.5B, R^2 = 0.987). Additionally, the size distributions matched well between VDC CTCs and IF CTCs (Fig. 4.5C), suggesting that the large, deformable population of cells from VDC are indeed CTCs.

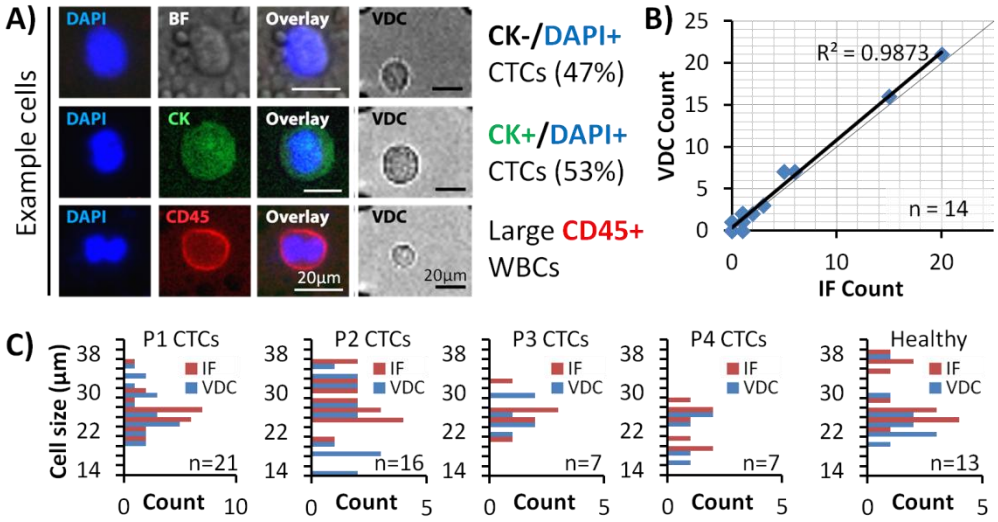

Figure 4.5: Comparisons of VDC with IF. (A) Similar to Vortex HT, VDC captured CTCs which stained both positive and negative for CK, as well as large white blood cells. **(B)** The number of CTCs defined from VDC matches closely with the number enumerated with conventional IF techniques. **(C)** The size distributions of CTCs from each patient matched closely between VDC and IF. Large WBCs also matched in size distributions, as observed in one healthy patient (last graph).

Finally, enumeration plots reveal that VDC finds 93.8% of cancer patient samples positive for CTCs, whereas IF techniques find approximately 71.4% of samples positive for CTCs (Fig. 4.6). Comparing the well-defined thresholding of VDC, which factors in both size and deformability, to the thresholding of IF, the use of biophysical cutoffs may thus be a more effective method for defining CTCs and distinguishing between cancer and healthy samples. Moreover, the VDC technique may be a more effective method than IF for CTC enumeration. Further long-term studies with more patient samples may be needed to support these preliminary findings.

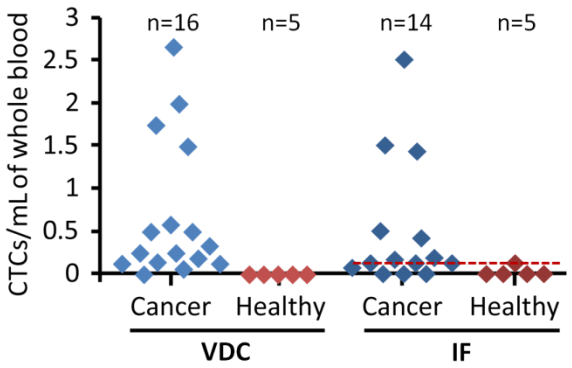

Figure 4.6: Enumeration of CTCs with VDC and IF. Biophysical enumeration of CTCs from 16 stage IV cancer samples revealed a 93.8% positive test rate, compared with a 71.4% positive rate for the gold standard IF technique.

Concluding remarks

Despite the ability for Vortex HT to isolate CTCs by size, classifying cells by cell diameter alone is insufficient to identify CTCs, as observed by the presence of large non-CTCs found in healthy samples. VDC technology factors both size and deformability of cells in a truly label-free, automatable, and sensitive method that may rapidly isolate and enumerate CTCs within 1 hr from receipt of a patient sample, while only requiring one blood dilution preparation step. The number of released CTCs is determined without the need for cell fixation, staining, or other processes that would damage the output sample, allowing it to be usable for further downstream analysis, such as genetic tests, drug screening, cytopathology, and other clinical applications. Further analysis of patient CTC mechanical properties may reveal physical phenotype distributions that better correlate to patient state than simple enumeration. Moreover, the transient responses and fluctuations of each cell at the flow junction provides over 15 other morphological parameters that may be biologically informative, and studies of these parameters may further expand the potential of biophysics as patient prognostic and diagnostic indicators. Finally, the demonstration of Vortex CTC enrichment and coupling to other technologies may prove useful for linking to other microfluidic platforms for other modes of single-cell analyses [10].

References

[1] Darling EM, Di Carlo D. High-Throughput Assessment of Cellular Mechanical Properties. *Annu Rev Biomed Eng*. 2015;17:150720185452003.

[2] Wolf-Ruprecht Wiedemeyer, Dongping Qi, Navjot Kaur Gill, Chintda Santiskulvong, Oliver Dorigo, JianYu Rao, Barbie Taylor-Harding, Amy C. Rowat. Parallel microfiltration (PMF): A novel method to screen cell mechanotype. [abstract]. In: Proceedings of the 106th Annual Meeting of the American Association for Cancer Research; 2015 Apr 18-22; Philadelphia, PA. Philadelphia (PA): AACR; *Cancer Res* 2015;75(15 Suppl):Abstract nr 226. doi:10.1158/1538-7445.AM2015-226

[3] Byun S, Son S, Amodei D, Cermak N, Shaw J, Kang JH, et al. Characterizing deformability and surface friction of cancer cells. *Proc Natl Acad Sci* USA. 2013;110:7580–5.

[4] Otto O, Rosendahl P, Mietke A, Golfier S, Herold C, Klaue D, et al. Real-time deformability cytometry: on-the-fly cell mechanical phenotyping. *Nat Methods*. 2015;12.

[5] Dudani JS, Gossett DR, Tse HTK, Di Carlo D. Pinched-flow hydrodynamic stretching of single-cells. *Lab Chip*. 2013;13:3728–34.

[6] Yang T, Paiè P, Nava G, Bragheri F, Vazquez RM, Minzioni P, et al. An integrated optofluidic device for single-cell sorting driven by mechanical properties. *Lab Chip*. Royal Society of Chemistry; 2015;15:1262–6.

[7] Qin X, Park S, Duffy SP, Matthews K, Ang RR, Todenhöfer T, et al. Size and deformability based separation of circulating tumor cells from castrate resistant prostate cancer patients using resettable cell traps. *Lab Chip*. Royal Society of Chemistry; 2015;15:2278–86.

[8] Gossett DR, Tse HTK, Lee S a, Ying Y, Lindgren AG, Yang OO, et al. Hydrodynamic stretching of single cells for large population mechanical phenotyping. *Proc Natl Acad Sci* U S A. 2012;109:7630–5.

[9] Tse HTK, Gossett DR, Moon YS, Masaeli M, Sohsman M, Ying Y, et al. Quantitative diagnosis of malignant pleural effusions by single-cell mechanophenotyping. *Sci Transl Med*. 2013;5:212ra163.

[10] Qi D, Hoelzle DJ, Rowat a. C. Probing single cells using flow in microfluidic devices. *Eur Phys J Spec Top*. 2012;204:85–101.

Chapter 5: Concluding Remarks

The Vortex platform has particular practical advantages. *Processing time:* A 7.5 mL whole blood sample can be processed in less than 20 mins, as compared to >2 hrs for many competing technologies, including CellSearch, MagSweeper, CTC-HB Chip, and Abnova, among others. *Wide applicability:* Vortex trapping is not restricted to blood and pleural effusions, as other bodily fluids may potentially be processed, including urine and perotineal fluids. Cancer cells can also be isolated independently of marker expression, suggesting the ability to accommodate a large range of tumor cell types, including cells of non-epithelial origin like melanoma or cells undergoing EMT. *Purity:* High purity is generally challenging because of a high background of WBCs adhering to coated surfaces or filter membranes. When using spiked samples, Vortex trapping routinely achieves a purity of ~80%, which is close to an order of magnitude greater than other high throughput inertial microfluidic technologies, such as the CTC-iChip and CTChip (Clearbridge Biomedics). *Efficiency:* While the efficiency of Vortex trapping may be considered relatively low compared to other techniques, it is improved with serial processing (up to 80% efficiency). Additional capture may be achieved by processing a larger blood volume (compared to the restrictions of ~1 mL for some current filter-based approaches). *Concentration and viability:* Importantly, no matter the volume processed, enriched cells are free, non-fixed, viable, and collected in a small 200 μL final suspension, while many continuous flow approaches result in highly dilute volumes that may be unsuitable for downstream assays.

The enriched tumor cells outputted from the Vortex platform may be applied to many clinical applications. As demonstrated, having access to pure DTCs from pleural effusions may aid cytopathology and genetic analyses, and access to CTCs from blood is beneficial for

immunofluorescence and mechanophenotyping. Rare cell isolation provides additional clinical opportunities, including FISH staining, RNA/DNA sequencing, single cell Western blotting, and other established techniques that may assist patient treatments (immunotherapy, response to chemotherapy, targeted drug delivery, etc.). On a more biological perspective, cells may also potentially be cultured or screened against a panel of therapeutic agents to learn more about cancers and discover new modes of cancer treatment. Moreover, the ability for the Vortex platform to be coupled to downstream techniques with minimal cell loss may also foster DTC analyses in next generation microfluidic devices, such as in the use of digital droplet assays or other modes of cellular quantitation.

The straightforward workflow and simplistic design makes Vortex technology a viable candidate as a commercial healthcare tool, since automation and cost are key considerations for successful adoption and implementation in a clinical setting. Vortex trapping employs passive fluid physics to selectively and rapidly collect larger cells in laminar fluid microvortices without complex high-resolution features, instrumentation, or surface chemistry. Consequently, the cost of an injection-molded chip and the per-sample cost for the pressure control system to process samples is expected to be much lower than existing commercial assays (e.g. ~$500 per test for the CellSearch system). Considering the set of capabilities discussed, the simplicity of vortex trapping can aid widespread adoption from both clinicians and cancer biologists alike, and may hopefully beneficially impact the cancer healthcare field.